# TECH BRIEFS

## NATIONAL AERONAUTICS AND SPACE ADMINISTRATION

Technology Focus

Electronics/Computers

Software

Materials

Mechanics/Machinery

Manufacturing

Bio-Medical

Physical Sciences

Information Sciences

Books and Reports

# INTRODUCTION

Tech Briefs are short announcements of innovations originating from research and development activities of the National Aeronautics and Space Administration. They emphasize information considered likely to be transferable across industrial, regional, or disciplinary lines and are issued to encourage commercial application.

## Availability of NASA Tech Briefs and TSPs

Requests for individual Tech Briefs or for Technical Support Packages (TSPs) announced herein should be addressed to

**National Technology Transfer Center**
Telephone No. **(800) 678-6882** or via World Wide Web at **www.nttc.edu**

Please reference the control numbers appearing at the end of each Tech Brief. Information on NASA's Innovative Partnerships Program (IPP), its documents, and services is also available at the same facility or on the World Wide Web at **http://www.nasa.gov/offices/ipp/network/index.html**

Innovative Partnerships Offices are located at NASA field centers to provide technology-transfer access to industrial users. Inquiries can be made by contacting NASA field centers listed below.

# NASA Field Centers and Program Offices

**Ames Research Center**
Lisa L. Lockyer
(650) 604-1754
lisa.l.lockyer@nasa.gov

**Dryden Flight Research Center**
Gregory Poteat
(661) 276-3872
greg.poteat@dfrc.nasa.gov

**Glenn Research Center**
Kathy Needham
(216) 433-2802
kathleen.k.needham@nasa.gov

**Goddard Space Flight Center**
Nona Cheeks
(301) 286-5810
nona.k.cheeks@nasa.gov

**Jet Propulsion Laboratory**
Andrew Gray
(818) 354-3821
gray@jpl.nasa.gov

**Johnson Space Center**
information
(281) 483-3809
jsc.techtran@mail.nasa.gov

**Kennedy Space Center**
David R. Makufka
(321) 867-6227
david.r.makufka@nasa.gov

**Langley Research Center**
Brian Beaton
(757) 864-2192
brian.f.beaton@nasa.gov

**Marshall Space Flight Center**
Jim Dowdy
(256) 544-7604
jim.dowdy@msfc.nasa.gov

**Stennis Space Center**
Ramona Travis
(228) 688-3832
ramona.e.travis@nasa.gov

**Carl Ray, Program Executive**
Small Business Innovation
Research (SBIR) & Small
Business Technology
Transfer (STTR) Programs
(202) 358-4652
carl.g.ray@nasa.gov

**Doug Comstock, Director**
Innovative Partnerships
Program Office
(202) 358-2560
doug.comstock@nasa.gov

# TECH BRIEFS

## NATIONAL AERONAUTICS AND SPACE ADMINISTRATION

# ✿ Sprag Handle Wrenches

**These wrenches could supplant conventional ratcheting wrenches.**

*Goddard Space Flight Center, Greenbelt, Maryland*

Sprag handle wrenches have been proposed for general applications in which conventional pawl-and-ratchet wrenches and sprag and cam "clickless" wrenches are now used. Sprag handle wrenches are so named because they would include components that would function both as parts of handles and as sprags (roller locking/unlocking components). In comparison with all of the aforementioned conventional wrenches, properly designed sprag handle wrenches could operate with much less backlash; in comparison with the con-ventional clickless wrenches, sprag handle wrenches could be stronger and less expensive (because the sprags would be larger and more easily controllable than are conventional sprags and cams).

A basic sprag handle wrench, shown in the upper part of the figure, would include the following parts:
• A frame that would constitute both the drive-head housing and part of the handle,
• A drive that would rotate freely within the drive-head housing except when engaged by sprags,
• An outer sprag that would constitute the rest of the handle, and
• An inner sprag that would engage the outer sprag at its outer end and the drive head at its inner end.

The frame would include a gap, into which the two sprags could be placed. Taken together, the inner sprag, the drive-head housing, and the drive would constitute the drive head. The inner and outer sprags would act as a roller-lock-ing/unlocking pair that would afford low-backlash ratcheting, as described below.

Omitted from the figure for the sake of clarity are gear-tooth-based roller sur-faces, on the sprags and in the frame, that would ensure the proper alignment and engagement between the sprags, be-tween the outer sprag and frame, and between the inner sprag and the drive. These surfaces would be such that (1) in preparation for applying torque, the op-erator could bring the ends of the sprags into contact with each other and with the frame and drive, by twisting the outer sprag slightly clockwise and (2) in preparation for free rotation for ratchet-ing to the starting position for the next torque-application stroke, the operator could relieve the contact forces on the sprags by twisting the outer sprag slightly counterclockwise.

In clockwise torquing, depicted schematically in the lower part of the fig-ure, the operator would push or pull on the outer-sprag portion of the handle in a clockwise direction; this action would jam the inner and outer sprags together



**TOP, SIDE AND SECTIONAL VIEWS**

**SCHEMATIC TOP VIEW ILLUSTRATING PRINCIPLE OF OPERATION**
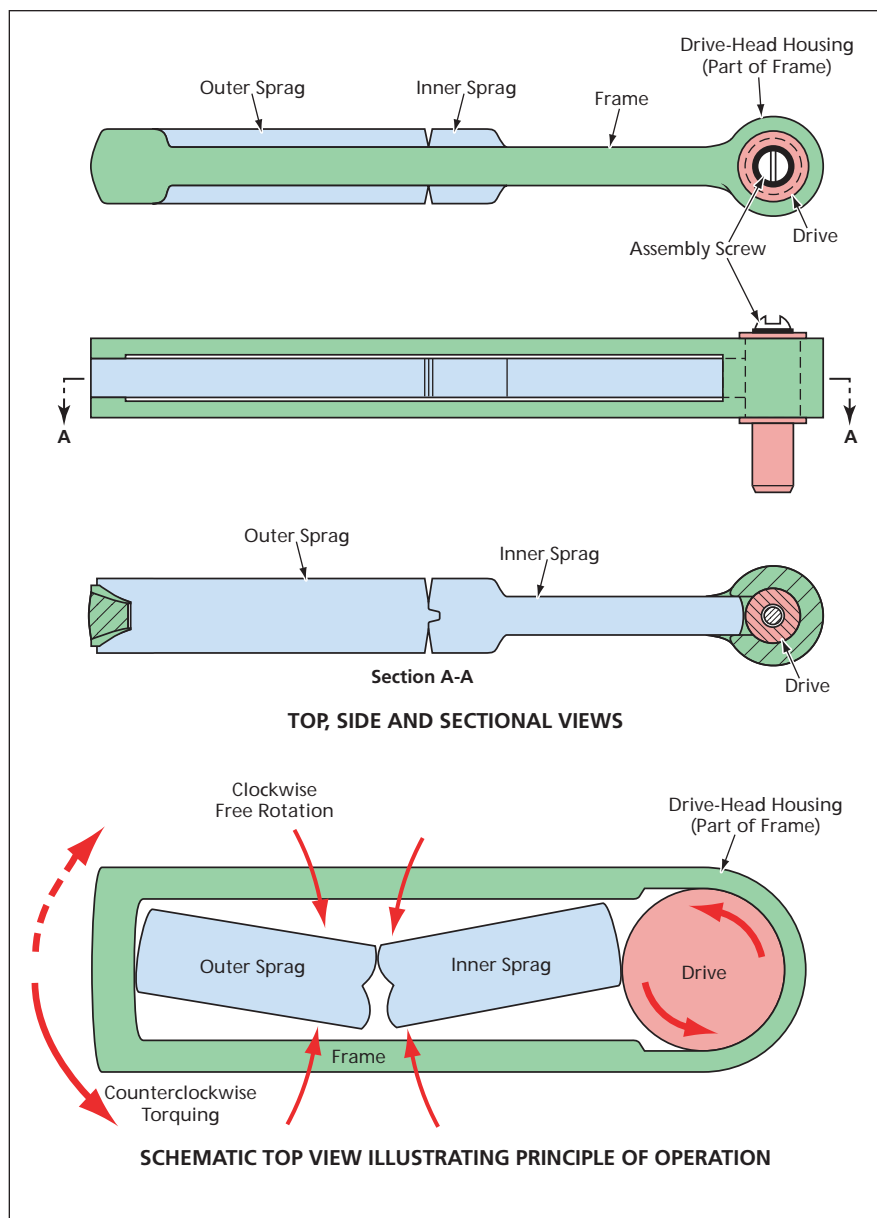
A **Basic Sprag Handle Wrench** would be a low-backlash, "clickless" ratcheting wrench that would offer advantages over conventional pawl-and-ratchet, sprag, and cam wrenches — essential when working in tight places.

between the frame at the outer end and the drive at the inner end. The jamming of the inner sprag against the drive would prevent rotation of the drive relative to the drive housing, so that clockwise torque would be exerted on the drive. At the end of the clockwise torque-application stroke, the operator would twist the outer sprag to relieve the contact forces as described above. Then by exerting a small counterclockwise force on the outer-sprag portion of the handle, the operator could further unjam the sprags to complete the disengagement with the drive, and turn the handle counterclockwise to the starting position for the next clockwise torque-application stroke. Except for reversal of the directions of all forces, torques, and rotations, counterclockwise ttorquing and ratcheting would be the same as in the clockwise case described above.

# ⚙ Miniature Low-Mass Drill Actuated by Flextensional Piezo Stack

**This extremely small impact drill can be used for testing soil for toxic chemicals, and other analytical tests.**

*NASA's Jet Propulsion Laboratory, Pasadena, California*

Recent experiments with a flextensional piezoelectric actuator have led to the development of a sampler with a bit that is designed to produce and capture a full set of sample forms including volatiles, powdered cuttings, and core fragments.

The flextensional piezoelectric actuator is a part of a series of devices used to amplify the generated strain from piezoelectric actuators. Other examples include stacks, bimorphs, benders, and cantilevers. These devices combine geometric and resonance amplifications to produce large stroke at high power density. The operation of this sampler/drill was demonstrated using a 3×2×1-cm actuator weighing 12 g using power of about 10-W and a preload of about 10 N. A limestone block was drilled to a depth of about 1 cm in five minutes to produce powdered cuttings.

It is generally hard to collect volatiles from random surface profiles found in rocks and sediment, powdered cuttings, and core fragments. Toward the end of collecting volatiles, the actuator and the bit are covered with bellows-shaped shrouds to prevent fines and other debris from reaching the analyzer. A tube with a miniature bellows (to provide flexibility) is connected to the bit and directs the flow of the volatiles to the analyzer. Another modality was conceived where the hose is connected to the bellows wall directly to allow the capture of volatiles generated both inside and outside the bit. A wide variety of commercial bellows used in the vacuum and microwave industries can be used to design the volatiles' capture mechanism.

The piezoelectric drilling mechanism can potentially be operated in a broad temperature range from about −200 to <450 ºC. The actuators used here are similar to the actuators that are currently baselined to fly as part of the inlet funnel shaking mechanism design of MSL (Mars Science Laboratory). The space qualification of these parts gives this drill a higher potential for inclusion in a future mission, especially when considering its characteristics of low mass, small size, low power, and low axial loads for sampling.
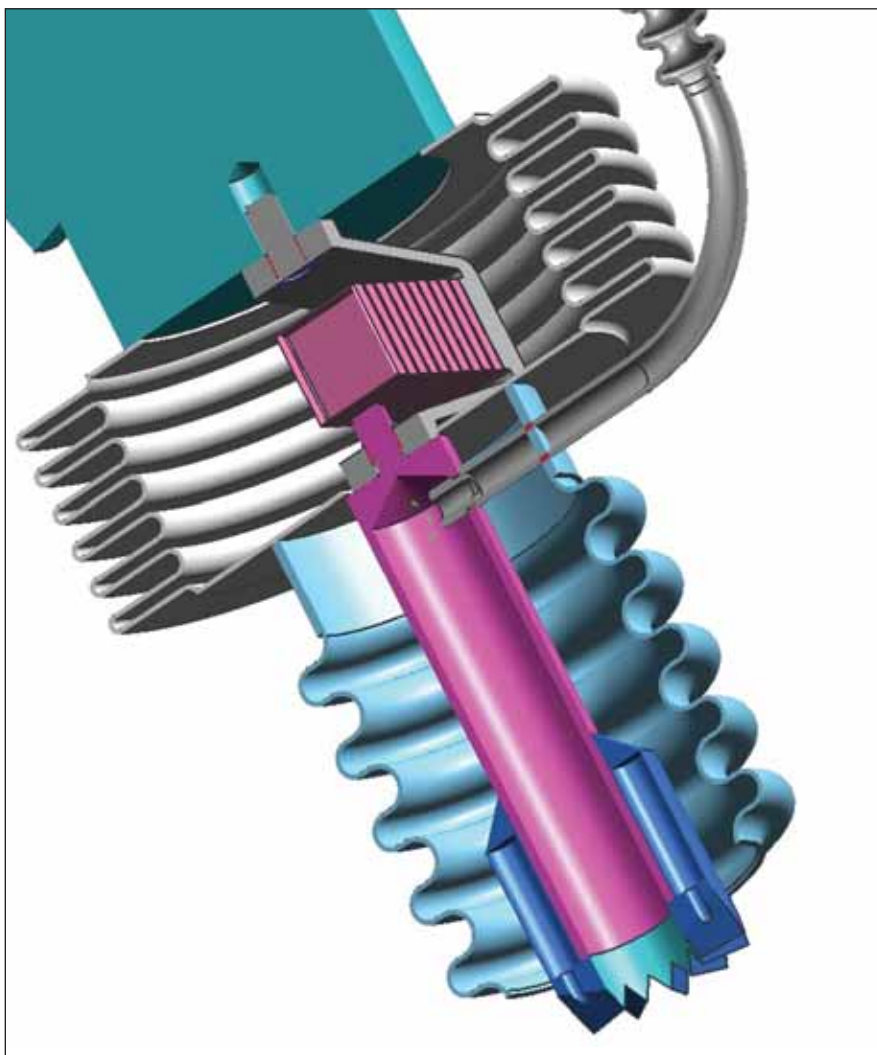


The **Miniature Drill**, the bit, and the covering of both the actuator and bit using bellows are shown. The tube with bellows also is shown.

Such a tiny penetrator can be integrated with instruments for life and water detection as well as materials characterization for planetary applications. It is also a useful tool for gaining subsurface access, an exploration goal that is an essential element of future missions. Terrestrially speaking, this tool has applications with regard to testing soil for toxic chemicals, the presence of mois-

ture, and various other analytical tests.

# Inline Electrical Connector Mate/Demate Pliers

## These pliers are designed for use in tight spaces and recessed electrical panels.

*John F. Kennedy Space Center, Florida*

Military and aerospace industries use Mil-Spec type electrical connections on bulkhead panels that require inline access for mate and demate operations. These connectors are usually in tight proximity to other connectors, or recessed within panels. The pliers described here have been designed to work in such tight spaces, and consist of a mirrored set of parallel handles, two cross links, two return springs, and replaceable polyurethane-coated end effectors. The polyurethane eliminates metal-to-metal contact and provides a high-friction surface between the jaw and the connector.

Operationally, the user would slide the pliers over the connector shell until the molded polyurethane lip makes contact with the connector shell edge. Then, by squeezing the handles, the end effector jaws grip the connector shell, allowing the connector to be easily disconnected by rotating the pliers. Mating the connector occurs by reversing the prescribed procedure, except the connector shell is placed into the jaws by hand. The molded lip within the jaw allows the user to apply additional force for difficult-to-mate connectors.

Handle design has been carefully examined to maximize comfort, limit weight, incorporate tether locations, and improve ergonomics. They have been designed with an off-axis offset for wiring harness clearance, while placing the connector axis of rotation close to the user's axis of wrist rotation. This was done to eliminate fatigue during multiple connector panel servicing. To limit handle opening width, with user ergonomics in mind, the pliers were designed using a parallel jaw mechanism. A cross-link mechanism was used to com-



The **Mate/Demate Pliers**, shown in their open and closed configurations, feature cross-link springs to ensure they remain in the open position until adequate force is applied to close them.

plete this task, while ensuring smooth operation.

Forward slides allow the links to change position during opening and closing. Springs were added to the cross links to ensure that the pliers remain in the open position until adequate force is applied to close them. The jaw end effectors can be easily removed and replaced to accommodate a range of connector sizes. Because the pliers were designed with the intent of reducing the

risk of foreign object debris (FOD), the end effectors contain two capturing features. They are held in place by means of two captive screw retainers while a secondary detent feature holds the jaws in case the screw retainers fail or become loose.

# Adaptable Holders for Arc-Jet Screening Candidate Thermal Protection System Repair Materials

*Lyndon B. Johnson Space Center, Houston, Texas*

Reusable holders have been devised for evaluating high-temperature, plasma-resistant re-entry materials, especially fabrics. Typical material samples tested support thermal-protection-system damage repair requiring evaluation prior to re-entry into terrestrial atmosphere. These tests allow evaluation of each material to withstand the most severe predicted re-entry conditions.

In pursuit of this purpose, the holders are capable of supporting the material samples in a stagnation orientation (normal to the flow) with respect to the impinging plasma flow. The holder design allows rapid installation and change-out of 2.8 in. ($\approx$ 71 mm) diameter samples and can accommodate sample thicknesses from fabrics to more than 0.5 in. ($\approx$ 13 mm). Each holder consists of an interlocking set of rings, constructed of silicon carbide coated graphite, that clamp together concentrically in such a manner as to restrain the sample during a test. The sample is mounted in front of a washerlike backing plate to simulate the repair of a damaged section of reinforced carbon-carbon (RCC), such as that used on the Space Shuttle Orbiter.

*This work was done by Joe Riccio of Johnson Space Center and Jim D. Milhoan of Lockheed Martin Corp. Further information is contained in a TSP (see page 1).MSC-24109-1*

# Seal With Integrated Shroud for Androgynous Docking and Berthing
## Seal prevents gas leakage between the pressurized module and its external environment.

*John H .Glenn Research Center, Cleveland, Ohio*

A specially configured seal system (see figure) has been developed and produced that provides a barrier to gas leakage between a pressurized module and its external environment. The seal system includes a shroud covering that both protects the sealing surface from its environment when not in use and retracts to expose the sealing surface when engaged. The seal system is constructed and arranged to mate with a replicate seal system or with a flat surface. When mated with a replicate seal system, the seal system functions when the two sealing surfaces are aligned or misaligned. The seal system can operate over a wide range of temperatures, limited only by the glass transition and melt temperatures of the material from which the sealing surface is manufactured.

*This work was done by Christopher C. Daniels of The University of Akron for Glenn Research Center. Further information is contained in a TSP (see page 1).*

In accordance with Public Law 96-517, the contractor has elected to retain title to this invention. Inquiries concerning rights for its commercial use should be addressed to:

Office of Technology Transfer
The University of Akron
Akron, Ohio 44325-2103
(330) 972-7840
Email: uarf@uakron.edu

Refer to LEW-18442-1, volume and number of this NASA Tech Briefs issue, and the
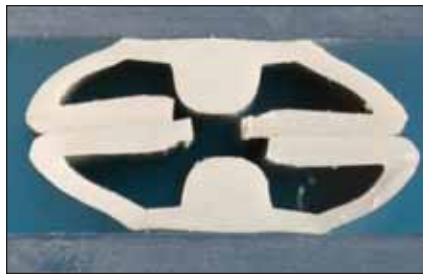
The **Shroud Covering** protects the sealing surface from the environment when not in use (top) and retracts when mated (bottom).

# Locking Nut With Stress-Distributing Insert

*Lyndon B. Johnson Space Center, Houston, Texas*

An improved locking nut comprises (1) an internally threaded shell, partly resembling a conventional nut, that can be engaged by a wrench or other tool, and (2) an internally and externally threaded insert that engages the threads of the shell and a bolt. Whereas some prior locking nuts are plated over their entire surfaces for lubrication and prevention of galling caused by engagement of threaded surfaces, this nut includes plating (silver or other soft material) only on the threaded surfaces of the insert, which, during engagement, are enclosed. The elimination of external plating reduces the likelihood of contaminating adjacent equipment.

The insert makes an interference fit

with the bolt thread, helping to lock the shell against loosening during vibration. In response to bolt tension upon tightening, the insert undergoes slight elongation that helps distribute the tension along the full length of thread engagement. The locking nut helps to dissipate vibrational energy through microscopic frictional rubbing between the threads of the insert and the threads of the shell. The soft plating may contribute to damping of vibrations. Rounding of the outer end of the shell reduces the potential for damage to nearby equipment or injury to nearby persons.

*This work was done by Rahmatollah F. Toosky and Scott Forest of McDonnell Douglas Corp. for Johnson Space Center. Further information is contained in a TSP (see page 1).*

# Digitally Controlled Slot Coupled Patch Array

*John H. Glenn Research Center, Cleveland, Ohio*

A four-element array conformed to a singly curved conducting surface has been demonstrated to provide 2 dB axial ratio of 14 percent, while maintaining VSWR (voltage standing wave ratio) of 2:1 and gain of 13 dBiC. The array is digitally controlled and can be scanned with the LMS Adaptive Algorithm using the power spectrum as the objective, as well as the Direction of Arrival (DoA) of the beam to set the amplitude of the power spectrum. The total height of the array above the conducting surface is 1.5 inches (3.8 cm).

A uniquely configured microstrip-coupled aperture over a conducting surface produced supergain characteristics, achieving 12.5 dBiC across the 2-to-2.13-GHz and 2.2-to-2.3-GHz frequency bands. This design is optimized to retain VSWR and axial ratio across the band as well. The four elements are uniquely configured with respect to one another for performance enhancement, and the appropriate phase excitation to each element for scan can be found either by analytical beam synthesis using the genetic algorithm with the measured or simulated far field radiation pattern, or an adaptive algorithm implemented with the digitized signal.

The commercially available tuners and field-programmable gate array (FPGA) boards utilized required precise phase coherent configuration control, and with custom code developed by Nokomis, Inc., were shown to be fully functional in a two-channel configuration controlled by FPGA boards. A four-channel tuner configuration and oscilloscope configuration were also demonstrated although algorithm post-processing was required.

*This work was done by Thomas D'Arista and Jerry Pauly of Nokomis, Inc. for Glenn Research Center. Further information is contained in a TSP (see page 1).*

*Inquiries concerning rights for the commercial use of this invention should be addressed to NASA Glenn Research Center, Innovative Partnerships Office, Attn: Steven Fedor, Mail Stop 4–8, 21000 Brookpark Road, Cleveland, Ohio 44135. Refer to LEW-18540-1.*

# Reconfigurable Robust Routing for Mobile Outreach Network

**The envisioned lunar network comprises many heterogeneous assets integrated by various protocols and technologies.**

*John H. Glenn Research Center, Cleveland, Ohio*

The Reconfigurable Robust Routing for Mobile Outreach Network (R3MOON) provides advanced communications networking technologies suitable for the lunar surface environment and applications. The R3MOON technology is based on a detailed concept of operations tailored for lunar surface networks, and includes intelligent routing algorithms and wireless mesh network implementation on AGNC's Coremicro Robots.

The product's features include an integrated communication solution incorporating energy efficiency and disruption-tolerance in a mobile *ad hoc* network, and a real-time control module to provide researchers and engineers a convenient tool for reconfiguration, investigation, and management.

A new routing protocol extends existing routing methods such that more alternate routes can be found between the source and the destination. This leads to better packet delivery rate as well as larger extent of delivery. Alternate routes can also be used for route optimization wherein the most energy efficient route is chosen. The criterion of energy efficiency can be readily reconfigured to accommodate different design objectives and network requirements.

When disruption occurs, a data buffering mechanism is established so that the undeliverable packet is stored at a dynamically selected storage node while awaiting redelivery. Since the undeliverable packet is not discarded but buffered, robustness is achieved. A proper storage node is chosen by considering its buffer space, battery power, and location.

A hardware prototype network is developed based on AGNC's product solutions such as Coremicro Robot and Coremicro 40 GIS. The multi-robot demonstration scheme incorporates mesh and relay networking. With three network nodes, routing capability is tested, verified, and monitored on this platform with a real-time Coremicro 40 GIS based robot Operator Control Unit (OCU). Multimedia data is exchanged in the network through effective communication and routing, even upon disruption. When one of the direct links is disrupted, an alternative two-hop path can be used to accomplish the communication.

R3MOON offers the following novel features in a complete and comprehensive communication solution:

- Energy-efficient routing achieved through path selection. This approach is highly feasible and implementable.
- Disruption-tolerant routing achieved through data buffering and retransmission mechanism. This approach is also based on AODV (*ad hoc* on-demand distance vector) routing protocol. Retransmission from the storage node achieves more graceful packet discarding rate, faster restoration, and higher redelivery rate than retransmission from the source node.
- Implementation and performance demonstration through software and hardware realization. The simulation shows animation for the route discovery process, and validates the performance of the proposed method in vari-

ous simulated network settings.

• An actual implementation of a mesh network architecture that integrates network control and optimization functionalities. The integral approach combines communication, navigation, control, and other functions needed to perform the mission. Each network node (e.g., robot) houses modules such as robot control processor, sensor fusion processor, and image processor, which are all interconnected through a communication module. The communication module connects all the nodes in the network. The configuration can be customized for designer's needs such as reduction of power consumption or simplification of wiring. In the higher level of the R3MOON architecture, a human/machine interface is embedded for executing AGNC's 4D-GIS and for monitoring and management of the network.

• A communication module that can be configured with different routing algorithms to run the mesh network. Both proactive [e.g., OLSR (Optimized Link State Routing)] and reactive (e.g., AODV) based routing protocols can be used in the module. A mesh wireless network with optimized routing algorithms enhances system reliability and performance.

# Fiber-Scanned Microdisplays

*Lyndon B. Johnson Space Center, Houston, Texas*

Helmet- and head-mounted display systems, denoted fiber-scanned microdisplays, have been proposed to provide information in an "augmented reality" format (meaning that the information would be optically overlaid on the user's field of view). A system of this type would include laser diodes feeding light into the input ends of optical fibers. The output ends of the fibers would be vibrated in prescribed patterns (scanned), in synchronism with excitation of the laser diodes, to trace out the patterns to be displayed. Lenses would form virtual images of the patterns and project the images directly (or by reflection) into the viewer's eyes.

The effective object distance of the images could be set to approximate the distances of other objects in the field of view, so that the viewer need not refocus to view the display. The display units could be positioned to present the displays at the margin of the field of view, thereby minimizing distraction when the user needs to concentrate attention elsewhere. Alternatively, the display units could be mounted so that a turn of the eye or a slight turn of the head from a nominal straight-ahead orientation would be necessary for viewing the displays.

# Reconfigurable Fault Tolerance for FPGAs

**FPGAs can be reconfigured to provide higher capacity or fault-tolerant redundancy.**

*Lyndon B. Johnson Space Center, Houston, Texas*

The invention allows a field-programmable gate array (FPGA) or similar device to be efficiently reconfigured in whole or in part to provide higher capacity, non-redundant operation. The redundant device consists of functional units such as adders or multipliers, configuration memory for the functional units, a programmable routing method, configuration memory for the routing method, and various other features such as block RAM, I/O (random access memory, input/output) capability, dedicated carry logic, etc. The redundant device has three identical sets of functional units and routing resources and majority voters that correct errors. The configuration memory may or may not be redundant, depending on need. For example, SRAM-based FPGAs will need some type of radiation-tolerant configuration memory, or they will need triple-redundant configuration memory. Flash or anti-fuse devices will generally not need redundant configuration memory. Some means of loading and verifying the configuration memory is also required. These are all components of the pre-existing redundant FPGA.

This innovation modifies the voter to accept a MODE input, which specifies whether ordinary voting is to occur, or if redundancy is to be split. Generally, additional routing resources will also be required to pass data between sections of the device created by splitting the redundancy. In redundancy mode, the voters produce an output corresponding to the two inputs that agree, in the usual fashion. In the split mode, the voters select just one input and convey this to the output, ignoring the other inputs. In a dual-redundant system (as opposed to triple-redundant), instead of a voter, there is some means to latch or gate a state update only when both inputs agree. In this case, the invention would require modification of the latch or gate so that it would operate normally in redundant mode, and would separately latch or gate the inputs in non-redundant mode.

For fault tolerance, it is assumed that only one fault will occur within a voting group within one voting cycle, and thus, the fault can be eliminated by majority voting. Three voters are often used, providing three values to the next voting group, and so on, with the

entire device triplicated. The only connection between the three sections of the device is the voters. By changing the operation of the voters, the sections can operate independently. A system of triple-redundant voted configuration data (if needed, according to the configuration memory type) can be used to provide routing connections to allow communication between the sections. The ability to use hardware-based redundancy where needed in high-capacity applications may help avoid high development costs, difficult maintenance, and complex failure of firmware redundancy schemes.

*This work was done by Robert Shuler, Jr. of Johnson Space Center. Further information is contained in a TSP (see page 1).*

*This invention is owned by NASA, and a patent application has been filed. Inquiries concerning nonexclusive or exclusive license for its commercial development should be addressed to the Patent Counsel, Johnson Space Center, (281) 483-1003. Refer to MSC-24464-1.*

# Software

## MIRO Computational Model

A computational model calculates the excitation of water rotational levels and emission-line spectra in a cometary coma with applications for the Microwave Instrument for Rosetta Orbiter (MIRO). MIRO is a millimeter-submillimeter spectrometer that will be used to study the nature of cometary nuclei, the physical processes of outgassing, and the formation of the head region of a comet (coma). The computational model is a means to interpret the data measured by MIRO.

The model is based on the accelerated Monte Carlo method, which performs a random angular, spatial, and frequency sampling of the radiation field to calculate the local average intensity of the field. With the model, the water rotational level populations in the cometary coma and the line profiles for the emission from the water molecules as a function of cometary parameters (such as outgassing rate, gas temperature, and gas and electron density) and observation parameters (such as distance to the comet and beam width) are calculated.

*This work was done by Paul A. Von Allmen and Seungwon Lee of Caltech for NASA's Jet Propulsion Laboratory. Further information is contained in a TSP (see page 1).*

*This software is available for commercial licensing. Please contact Daniel Broderick of the California Institute of Technology at danielb@caltech.edu. Refer to NPO-46508.*

## Team Collaboration Software

The Ground Resource Allocation and Planning Environment (GRAPE 1.0) is a Web-based, collaborative team environment based on the Microsoft SharePoint platform, which provides Deep Space Network (DSN) resource planners' tools and services for sharing information and performing analysis. The foundation platform for GRAPE provides a number of communication and data-management mechanisms, which help planners communicate scheduling issues, including document management, security schemes, calendars, wikis, blogs, lists, issue tracking, discussion forums, workflow management, alerts/notifications, and configuration management.

Additionally, a set of "web parts" has been developed for DSN resource-allocation-specific analysis, including tools for managing ground asset and mission information; finding configuration codes; displaying, querying, and comparing schedules; analyzing mission coverage; checking for schedule conflicts; creating and submitting schedule change requests; and viewing and validating mission view periods. The methodology of web parts allows individual users to compose their own Web pages by picking the web parts they want to use on a Web page, rather than developers designing Web pages for users. This allows developers to focus more on functionality and less on appearance and integration, while users are empowered to compose Web pages for their immediate analysis and collaboration needs rather than waiting for another long development cycle for some new capability. GRAPE web parts, which connect to existing DSN middle-tier Web services for many computation and data access activities, support Service Oriented Architecture (SOA), and component-style development.

*This work was done by Yeou-Fang Wang, Mitchell Schrock, John R. Baldwin, and Chester S. Borden of Caltech for NASA's Jet Propulsion Laboratory. Further information is contained in a TSP (see page 1).*

*This software is available for commercial licensing. Please contact Daniel Broderick of the California Institute of Technology at danielb@caltech.edu. Refer to NPO-45988.*

## Comet Gas and Dust Dynamics Modeling

This software models the gas and dust dynamics of comet coma (the head region of a comet) in order to support the Microwave Instrument for Rosetta Orbiter (MIRO) project. MIRO will study the evolution of the comet 67P/Churyumov-Gerasimenko's coma system. The instrument will measure surface temperature, gas-production rates and relative abundances, and velocity and excitation temperatures of each species along with their spatial temporal variability. This software will use these measurements to improve the understanding of coma dynamics.

The modeling tool solves the equation of motion of a dust particle, the energy balance equation of the dust particle, the continuity equation for the dust and gas flow, and the dust and gas mixture energy equation. By solving these equations numerically, the software calculates the temperature and velocity of gas and dust as a function of time for a given initial gas and dust production rate, and a dust characteristic parameter that measures the ability of a dust particle to adjust its velocity to the local gas velocity.

The software is written in a modular manner, thereby allowing the addition of more dynamics equations as needed. All of the numerical algorithms are added in-house and no third-party libraries are used.

*This work was done by Paul A. Von Allmen and Seungwon Lee of Caltech for NASA's Jet Propulsion Laboratory. Further information is contained in a TSP (see page 1).*

*This software is available for commercial licensing. Please contact Daniel Broderick of the California Institute of Technology at danielb@caltech.edu. Refer to NPO-46507.*

## Online Planning Algorithm

AVA v2 software selects goals for execution from a set of goals that oversubscribe shared resources. The term "goal" refers to a science or engineering request to execute a possibly complex command sequence, such as image targets or ground-station downlinks.

Developed as an extension to the Virtual Machine Language (VML) execution system, the software enables on-board and remote goal triggering through the use of an embedded, dynamic goal set that can oversubscribe resources. From the set of conflicting goals, a subset must be chosen that maximizes a given quality metric, which in this case is strict priority selection. A goal can never be preempted by a lower priority goal, and high-level goals can be added, removed, or updated at any time, and the "best" goals will be selected for execution.

The software addresses the issue of re-planning that must be performed in a short time frame by the embedded system where computational resources are constrained. In particular, the algorithm addresses problems with well-defined goal requests without temporal flexibility that oversubscribes

available resources. By using a fast, incremental algorithm, goal selection can be postponed in a "just-in-time" fashion allowing requests to be changed or added at the last minute. Thereby enabling shorter response times and greater autonomy for the system under control.

*This work was done by Gregg R. Rabideau and Steve A. Chien of Caltech for NASA's Jet Propulsion Laboratory.*

*This software is available for commercial licensing. Please contact Daniel Broderick of the California Institute of Technology at danielb@caltech.edu. Refer to NPO-46503.*

## ⅀ AutoGNC Testbed

A simulation testbed architecture was developed and implemented for the integration, test, and development of a TRL-6 flight software set called Auto-GNC. The AutoGNC software will combine the TRL-9 Deep Impact AutoNAV flight software suite, the TRL-9 Virtual Machine Language (VML) executive, and the TRL-3 G-REX guidance, estimation, and control algorithms. The Auto-GNC testbed was architected to provide software interface connections among the AutoNAV and VML flight code written in C, the G-REX algorithms in MAT-LAB and C, stand-alone image rendering algorithms in C, and other Fortran algorithms, such as the OBIRON landmark tracking suite.

The testbed architecture incorporates software components for propagating a high-fidelity "truth" model of the environment and the spacecraft dynamics, along with the flight software components for onboard guidance, navigation, and control (GN&C). The interface allows for the rapid integration and testing of new algorithms prior to development of the C code for implementation in flight software.

This testbed is designed to test autonomous spacecraft proximity operations around small celestial bodies, moons, or other spacecraft. The software is baselined for upcoming comet and asteroid sample return missions. This architecture and testbed will provide a direct improvement upon the onboard flight software utilized for missions such as Deep Impact, Stardust, and Deep Space 1.

*This work was done by John M. Carson III, Andrew T. Vaughan, David S. Bayard, Joseph E. Riedel, and J. Balaram of Caltech for NASA's Jet Propulsion Laboratory.*

*The software used in this innovation is available for commercial licensing. Please contact Daniel Broderick of the California Institute of Technology at danielb@caltech.edu. Refer to NPO 46557.*

## ⅀ Optical Imaging and Radiometric Modeling and Simulation

OPTOOL software is a general-purpose optical systems analysis tool that was developed to offer a solution to problems associated with computational programs written for the James Webb Space Telescope optical system. It integrates existing routines into coherent processes, and provides a structure with reusable capabilities that allow additional processes to be quickly developed and integrated. It has an extensive graphical user interface, which makes the tool more intuitive and friendly.

OPTOOL is implemented using MATLAB with a Fourier optics-based approach for point spread function (PSF) calculations. It features parametric and Monte Carlo simulation capabilities, and uses a direct integration calculation to permit high spatial sampling of the PSF. Exit pupil optical path difference (OPD) maps can be generated using combinations of Zernike polynomials or shaped power spectral densities. The graphical user interface allows rapid creation of arbitrary pupil geometries, and entry of all other modeling parameters to support basic imaging and radiometric analyses.

OPTOOL provides the capability to generate wavefront-error (WFE) maps for arbitrary grid sizes. These maps are 2D arrays containing digital sampled versions of functions ranging from Zernike polynomials to combination of sinusoidal wave functions in 2D, to functions generated from a spatial frequency power spectral distribution (PSD). It also can generate optical transfer functions (OTFs), which are incorporated into the PSF calculation.

The user can specify radiometrics for the target and sky background, and key performance parameters for the instrument's focal plane array (FPA). This radiometric and detector model setup is fairly extensive, and includes parameters such as zodiacal background, thermal emission noise, read noise, and dark current. The setup also includes target spectral energy distribution as a function of wavelength for polychromatic sources, detector pixel size, and the FPA's charge diffusion modulation transfer function (MTF).

*This work was done by Kong Q. Ha of KDA Engineering; Michael W. Fitzmaurice of Swales Aerospace; and Gary E. Moiser, Joseph M. Howard, and Chi M. Le of Goddard Space Flight Center. Further information is contained in a TSP (see page 1).GSC-15720-1*

# Nearly Seamless Vacuum-Insulated Boxes

## Elimination of most seams would reduce leakage of heat.

*Lyndon B. Johnson Space Center, Houston, Texas*

A design concept, and a fabrication process that would implement the design concept, have been proposed for nearly seamless vacuum-insulated boxes that could be the main structural components of a variety of controlled-temperature containers, including common household refrigerators and insulating containers for shipping foods. In a typical case, a vacuum-insulated box would be shaped like a rectangular parallelepiped conventional refrigerator box having five fully closed sides and a hinged door on the sixth side. Although it is possible to construct the five-closed-side portion of the box as an assembly of five unitary vacuum-insulated panels, it is not desirable to do so because the relatively high thermal conductances of the seams between the panels would contribute significant amounts of heat leakage, relative to the leakage through the panels themselves. In contrast, the proposal would make it possible to reduce heat leakage by constructing the five-closed-side portion of the box plus the stationary portion (if any) of the sixth side as a single, seamless unit; the only remaining seam would be the edge seal around the door.

The basic cross-sectional configuration of each side of a vacuum-insulated box according to the proposal would be that of a conventional vacuum-insulated panel: a low-density, porous core mate-rial filling a partially evacuated space between face sheets. However, neither the face sheets nor the core would be conventional. The face sheets would be opposite sides of a vacuum bag. The core material would be a flexible polymer-modified silica aerogel of the type described in "Silica/Polymer and Silica/Polymer/Fiber Composite Aerogels" (MSC-23736) in this issue of *NASA Tech Briefs*. As noted in that article, the stiffness of this core material against compression is greater than that of prior aerogels. This is an important advantage because it translates to greater retention of thickness and, hence, of insulation performance when pressure is applied across the thickness, in particular, when the space between the face sheets is evacuated, causing the core material to be squeezed between the face sheets by atmospheric pressure.

Fabrication of a typical vacuum-insulated box according to the proposal would begin with fabrication of a cross-shaped polymer-modified aerogel blanket. The dimensions of the cross would be chosen so that (1) the central rectangular portion of the cross would form the core for the back of the box and (2) the arms of the cross could be folded 90° from the back plane to form the cores of the adjacent four sides of the box. Optionally, the blanket could include tabs for joining the folded sides of the blan-ket along mating edges and tabs that could serve as hinges for the door.

Vacuum bags in the form of similar five-sided boxes would be made of a suitable polymeric film, one bag to fit the outer core surface, the other to fit the inner core surface. By use of commercially available film-sealing equipment, these box-shaped bags would be seamed together to form a single vacuum bag encasing the box-shaped core. Also, a one-way valve would be sealed to the bag. Through this valve, the interior of the bag would be evacuated to a pressure between 1 and 10 torr (approximately between 0.13 and 1.3 kPa). The polymer-modified aerogel core material is known to perform well as a thermal insulator in such a partial vacuum.

*This work was done by Christopher J. Stepanian, Danny Ou, and Xiangjun Hu of Aspen Aerogels, Inc., for Johnson Space Center. Further information is contained in a TSP (see page 1).*

# Quick-Change Ceramic Flame Holder for High-Output Torches

## In addition to jet engine simulation, this technology can be used in torches for forging and pottery kilns.

*Langley Research Center, Hampton, Virginia*

Researchers at NASA's Langley Research Center have developed a new ceramic design flame holder with a service temperature of 4,000 °F (2,204 °C). The combination of high strength and high temperature capability, as well as a twist-lock mounting method to the steel burner, sets this flame holder apart from existing technology.

This design features the following:
• Enables about double the torch output without damaging the torch.
• Can operate at a higher temperature [4,000 °F (2,204 °C)] than stainless steel [1,600 °F (870 °C)].
• Allows the torch to be optimized for different applications (e.g., may use a mixing nozzle or a supersonic nozzle).
• Can be used with either venturi or forced draft burners.
• Is easily replaceable without tools.
• Operates without torch/holder rusting together after use.
• Permits a modified torch to still use a conventional flame holder.

- Uses a twist-lock attachment (an improvement over setscrews).

The high-output flame holder was developed in support of the U.S. Navy's efforts to design a jet engine simulator for infrared plume studies. Previous tests had shown that off-the-shelf components would melt or burn up in a short time. Given these design and performance criteria, NASA developed a ceramic flame holder that has a much longer life cycle and can be used with a variety of torches or burners. Where the stainless flame holders showed signs of oxidation, flaking after only three hours of testing, NASA's ceramic flame holder has over 150 hours and 200 cycles of use in a casting furnace, and soot marks are the only signs of use; there are no signs of deterioration. NASA expects the new technology to help enhance safety through increased reliability and flame control. The total cost of ownership is less due to decreased maintenance and improved efficiency.

*This work was done by Henry Haskin of Langley Research Center. For further information, contact the Langley Innovative Partnerships Office at (757) 864-8881. LAR-17502-1*

# Non-Pyrotechnic Zero-Leak Normally Closed Valve

*Goddard Space Flight Center, Greenbelt, Maryland*

This valve is designed to create a zero-leak seal in a liquid propulsion system that is a functional replacement for the normally closed pyrovalve. Unlike pyrovalves, Nitinol is actuated by simply heating the material to a certain temperature, called the transition temperature. Like a pyrovalve, before actuation, the upstream and downstream sections are separated from one another and from the external environment by closed welded seals. Also like pyrovalves, after actuation, the propellant or pressurant gas can flow without a significant pressure drop but are still separated from the external environment by a closed welded seal.

During manufacture, a Nitinol bar is compressed to 93 percent of its original length and fitted tightly into the valve. During operation, the valve is heated until the Nitinol reaches the transition temperature of 95 °C; the Nitinol "remembers" its previous longer shape with a very large recovery force causing it to expand and break the titanium parent metal seal to allow flow. Once open, the valve forever remains open.

The first prototype valve was designed for high pressure [5,000 psi (≈34.5 MPa)] and low flow, typical requirements for pressurant gas valves in liquid propulsion systems. It is possible to modify the dimensions to make low-pressure models or high-flow models, for use downstream of the propellant tanks.

This design is simpler, lower risk, and less expensive than the pyrovalve. Although the valve must be in a thermally controlled state (kept below 80 °C) to prevent premature actuation, the pyrovalves and electrically actuated initiators have far more taxing handling requirements.

*This work was done by Rebecca Gillespie of Goddard Space Flight Center. Further information is contained in a TSP (see page 1).*

*This invention is owned by NASA, and a patent application has been filed. Inquiries concerning nonexclusive or exclusive license for its commercial development should be addressed to the Patent Counsel, Goddard Space Flight Center, (301) 286-7351. Refer to GSC-15328-1.*

# Fast-Response-Time Shape-Memory-Effect Foam Actuators

## These actuators have application in variable-area chevrons and nozzles in jet aircraft.

*John H. Glenn Research Center, Cleveland, Ohio*

Bulk shape memory alloys, such as Nitinol or CuAlZn, display strong recovery forces undergoing a phase transformation after being strained in their martensitic state. These recovery forces are used for actuation. As the phase transformation is thermally driven, the response time of the actuation can be slow, as the heat must be passively inserted or removed from the alloy.

Shape memory alloy TiNi torque tubes have been investigated for at least 20 years and have demonstrated high actuation forces [3,000 in.-lb (≈340 N-m) torques] and are very lightweight. However, they are not easy to attach to existing structures. Adhesives will fail in shear at low-torque loads and the TiNi is not weldable, so that mechanical crimp fits have been generally used. These are not reliable, especially in vibratory environments. The TiNi is also slow to heat up, as it can only be heated indirectly using heater and cooling must be done passively. This has restricted their use to on-off actuators where cycle times of approximately one minute is acceptable.

Self-propagating high-temperature synthesis (SHS) has been used in the past to make porous TiNi metal foams. Shape Change Technologies has been able to train SHS derived TiNi to exhibit the shape memory effect. As it is an open-celled material, fast response times were observed when the material was heated using hot and cold fluids.
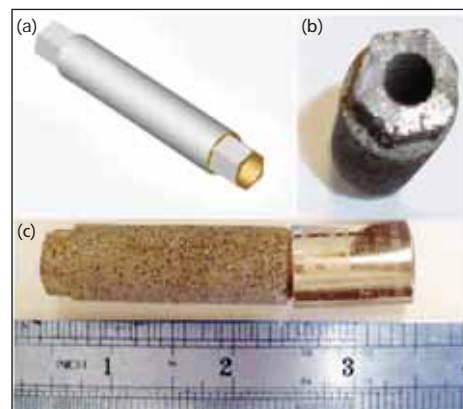


Figure: (a) **Schematic Representation of the TiNi Torque Tube**. The ends are integrated as hexagonal caps as shown in (b) and (c) shows a processed torque tube with a coupling at a representative length scale.

A methodology was developed to make the open-celled porous TiNi foams as a tube with integrated hexagonal ends, which then becomes a torsional actuator with fast response times. Under processing developed independently, researchers were able to verify torques of 84 in.-lb (≈9.5 N-m) using an actuator weighing 1.3 oz (≈37 g) with very fast (<1/16th of a second) initial response times when hot and cold fluids were used to facilitate heat transfer.

Integrated structural connections were added as part of the net shape process, eliminating the need for welding, adhesives, or mechanical crimping. Inexpensive net-shape processing was used, which reduces the cost of the actuator by over a factor of 10 over nonporous TiNi made by hot drawing of tube or electrical discharge machining.

By forming the alloy as an open-celled foam, the surface area for heat transfer is dramatically increased, allowing for much faster response times. The technology also allows for net-shape fabrication of the actuator, which allows for structural connections to be integrated into the actuator material, making these actuators significantly less expensive.

Commercial applications include actuators for concepts such as the variable-area chevron and nozzle in jet aircraft. Lightweight tube or rod components can be supplied to interested parties.

# Magnesium Diboride Current Leads

## The superconductor can be applied to cryogenic wiring.

*Goddard Space Flight Center, Greenbelt, Maryland*

A recently discovered superconductor, magnesium diboride ($MgB_2$), can be used to fabricate conducting leads used in cryogenic applications. Discovered to be superconducting in 2001, $MgB_2$ has the advantage of remaining superconducting at higher temperatures than the previously used material, NbTi. The purpose of these leads is to provide 2 A of electricity to motors located in a 1.3 K environment. The providing environment is a relatively warm 17 K. Requirements for these leads are to survive temperature fluctuations in the 5 K and 11 K heat sinks, and not conduct excessive heat into the 1.3 K environment. Test data showed that each lead in the assembly could conduct 5 A at 4 K, which, when scaled to 17 K, still provided more than the required 2 A.

The lead assembly consists of 12 steel-clad $MgB_2$ wires, a tensioned Kevlar support, a thermal heat sink interface at 4 K, and base plates. The wires are soldered to heavy copper leads at the 17 K end, and to thin copper-clad NbTi leads at the 1.3 K end. The leads were designed, fabricated, and tested at the Forschungszentrum Karlsruhe - Institut für Technische Physik before inclusion in Goddard's XRS (X-Ray Spectrometer) instrument onboard the Astro-E2 spacecraft.

A key factor is that $MgB_2$ remains superconducting up to 30 K, which means that it does not introduce joule heating as a resistive wire would. Because the required temperature ranges are 1.3–17 K, this provides a large margin of safety.

Previous designs lost superconductivity at around 8 K. The disadvantage to $MgB_2$ is that it is a brittle ceramic, and making thin wires from it is challenging. The solution was to encase the leads in thin steel tubes for strength. Previous designs were so brittle as to risk instrument survival.

$MgB_2$ leads can be used in any cryogenic application where small currents need to be conducted at below 30 K. Because previous designs would superconduct only at up to 8 K, this new design would be ideal for the 8–30 K range.

*This work was done by John Panek of Goddard Space Flight Center. For further information, contact the Goddard Innovative Partnerships Office at (301) 286-5810. GSC-15657-1*

# Polyimide Aerogels With Three-Dimensional Cross-Linked Structure

## These aerogels are suited for use as insulation as well as adsorbent beds for chemical separators, and as platforms for solid-state sensors.

*John H. Glenn Research Center, Cleveland, Ohio*

Polyimide aerogels with three-dimensional cross-linked structure are made using linear oligomeric segments of polyimide, and linked with one of the following into a 3D structure: trifunctional aliphatic or aromatic amines, latent reactive end caps such as nadic anhydride or phenylethynylphenyl amine, and silica or silsesquioxane cage structures decorated with amine. Drying the gels supercritically maintains the solid structure of the gel, creating a polyimide aerogel with improved mechanical properties over linear polyimide aerogels.

Lightweight, low-density structures are desired for acoustic and thermal insulation for aerospace structures, habitats, astronaut equipment, and aeronautic applications. Aerogels are a unique material for providing such properties because of their extremely low density and small pore sizes. How-

ever, plain silica aerogels are brittle. Reinforcing the aerogel structure with a polymer (X-Aerogel) provides vast improvements in strength while maintaining low density and pore structure. However, degradation of polymers used in cross-linking tends to limit use temperatures to below 150 ℃. Organic aerogels made from linear polyimide have been demonstrated, but gels shrink substantially during supercritical fluid extraction and may have lower use temperature due to lower glass transition temperatures.

The purpose of this innovation is to raise the glass transition temperature of all organic polyimide aerogel by use of tri-, tetra-, or poly-functional units in the structure to create a 3D covalently bonded network. Such cross-linked polyimides typically have higher glass transition temperatures in excess of

300–400 ℃. In addition, the reinforcement provided by a 3D network should improve mechanical stability, and prevent shrinkage on supercritical fluid extraction. The use of tri-functional aromatic or aliphatic amine groups in the polyimide backbone will provide such a 3D structure.

Alternatively, cross-linking of the polyimide can be carried out by capping long-chain oligomers with latent reactive end caps (nadic anhydride or phenylethynylphenylamine, for example). After supercritical fluid extraction, the cross-linking is carried out on a post-cure of the dried gels. In another embodiment, polyimide or polyamic acid can be capped with tri-alkoxy silanes, which can be co-reacted with small amounts of tetraalkoxy silanes to form regions of covalently bonded silica crosslinks. Alternately,

polysilsesquioxane cages decorated with surface amines can be co-reacted with anhydride capped polyimide/ polyamic acid.

Cross-linked polyimide aerogels with their high porosity, combined with higher strength, have excellent thermal as well as sound-insulating qualities. In addition, their high specific surface area (e.g. on the order of 200–1,000 $m^2/g$) should make them well suited for numerous applications, including as adsorbent beds for chemical separations, and as platforms for solid-state sensors.

*This work was done by Mary Ann B. Meador of Glenn Research Center. Further information is contained in a TSP (see page 1).*

*Inquiries concerning rights for the commercial use of this invention should be addressed to NASA Glenn Research Center, Innovative Partnerships Office, Attn: Steve Fedor, Mail Stop 4–8, 21000 Brookpark Road, Cleveland, Ohio 44135. Refer to LEW-18486-1.*

# Silica/Polymer and Silica/Polymer/Fiber Composite Aerogels

## These materials resist compression better than pure silica aerogels do.

*Lyndon B. Johnson Space Center, Houston, Texas*

Aerogels that consist, variously, of neat silica/polymer alloys and silica/polymer alloy matrices reinforced with fibers have been developed as materials for flexible thermal-insulation blankets. In comparison with prior aerogel blankets, these aerogel blankets are more durable and less dusty. These blankets are also better able to resist and recover from compression — an important advantage in that maintenance of thickness is essential to maintenance of high thermal-insulation performance. These blankets are especially suitable as core materials for vacuum-insulated panels and vacuum-insulated boxes of advanced, nearly seamless design. (Inasmuch as heat leakage at seams is much greater than heat leakage elsewhere through such structures, advanced designs for high insulation performance should provide for minimization of the sizes and numbers of seams.)

A silica/polymer aerogel of the present type could be characterized, somewhat more precisely, as consisting of multiply bonded, linear polymer reinforcements within a silica aerogel matrix. Thus far, several different polymethacrylates (PMAs) have been incorporated into aerogel networks to increase resistance to crushing and to improve other mechanical properties while minimally affecting thermal conductivity and density.

The polymethacrylate phases are strongly linked into the silica aerogel networks in these materials. Unlike in other organic/inorganic blended aerogels, the inorganic and organic phases are chemically bonded to each other, by both covalent and hydrogen bonds. In the process for making a silica/polymer alloy aerogel, the covalent bonds are introduced by prepolymerization of the methacrylate monomer with trimethoxysilylpropylmethacrylate, which serves as a phase cross-linker in that it contains both organic and inorganic monomer functional groups and hence acts as a connector between the organic and inorganic phases. Hydrogen bonds are formed between the silanol groups of the inorganic phase and the carboxyl groups of the organic phase. The polymerization process has been adapted to create interpenetrating PMA and silica-gel networks from monomers and prevent any phase separations that could otherwise be caused by an overgrowth of either phase.

Typically, the resulting PMA/silica aerogel, without or with fiber reinforcement, has a density and a thermal conductivity similar to those of pure silica aerogels. However, the PMA enhances mechanical properties. Specifically, flexural strength at rupture is increased to 102 psi ($\approx 0.7$ MPa), about 50 times the flexural strength of typical pure silica aerogels. Resistance to compression is also increased: Applied pressure of 17.5 psi ($\approx 0.12$ MPa) was found to reduce the thicknesses of several composite PMA/silica aerogels by only about 10 percent.

*This work was done by Danny Ou, Christopher J. Stepanian, and Xiangjun Hu of Aspen Aerogels, Inc., for Johnson Space Center. Further information is contained in a TSP (see page 1).*

*In accordance with Public Law 96-517, the contractor has elected to retain title to this invention. Inquiries concerning rights for its commercial use should be addressed to:*

*Aspen Aerogels, Inc.*
*30 Forbes Road, Building B*
*Northborough, MA 01532*
*Phone No.:(508) 691-1111*

*Refer to MSC-23736-1, volume and number of this* NASA Tech Briefs *issue, and the page number.*

# Alumina Paste Layer as a Sublimation Suppression Barrier for $Yb_{14}MnSb_{11}$

## This material can be applied to any thermoelectric couples requiring sublimation suppression.

*NASA's Jet Propulsion Laboratory, Pasadena, California*

Sublimation is a major cause of degradation of thermoelectric power generation systems. Most thermoelectric materials tend to have peak values at the temperature where sublimation occurs. A sublimation barrier is needed that is stable at operating temperatures, inert against thermoelectric materials, and able to withstand thermal cycling stress.

A porous alumina paste layer is suitable as a sublimation barrier for $Yb_{14}MnSb_{11}$. It can accommodate stress generated by the thermal expansion discrepancy between the suppression layer and thermoelectric materials. Sublimation suppression is achieved by filling pores naturally with $YbO_2$, a natural byproduct of sublimation. $YbO_2$ generated during the subli-
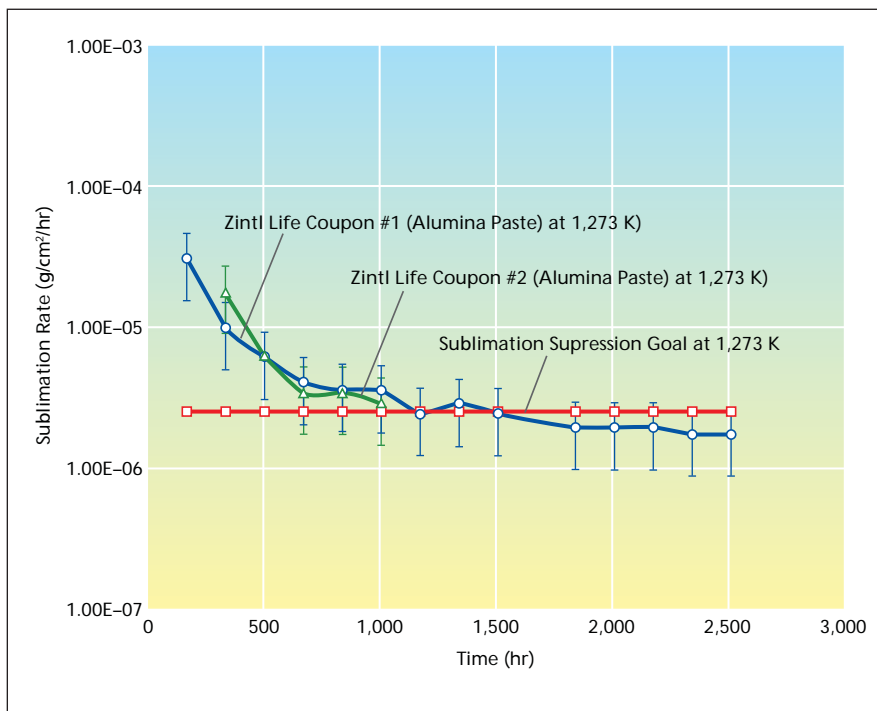
**Sublimation Rate Measurement** with $Yb_{14}MnSb_{11}$ coupons with an alumina paste layer. The sublimation rate at the beginning of life is rather high, but the rate decreases steadily and after 1,500 hours, the rate reaches below the goal and the filling of the pore during sublimation is believed to be the reason for the rate decrease with time.

mation of $Yb_{14}MnSb_{11}$ fills the porous structure of the alumina paste, causing sublimation to decrease with time as the pores become filled. During testing, it was found that application of this paste caused an initial ten-fold decrease in sublimation, but this factor increased with time. At 1,500 hours of burnout time at 1,273 K, the decrease in sublimation was measured as much as 1,000 times lower.

A commercial alumina paste was applied to $Yb_{14}MnSb_{11}$. Both elements were polished to remove oxidation, then the paste was applied to the $Yb_{14}MnSb_{11}$. The $Yb_{14}MnSb_{11}$ exhibited $2 \times 10^{-6}$ to $3 \times 10^{-6}$ g/cm$^2$ sublimation rate at 1,000 °C after initial burnout. With this rate, the sublimation barrier becomes suitable for 14-year operation, with less than 10 percent cross-section reduction at the hot side junction.

Using scanning electron microscope imaging, the alumina layer was found to be converted into a denser composite of alumina and ytterbia. This clogged, dense layer makes an effective sublimation barrier.

*This work was done by Jong-Ah Paik and Thierry Caillat of Caltech for NASA's Jet Propulsion Laboratory. Further information is contained in a TSP (see page 1).*

*In accordance with Public Law 96-517, the contractor has elected to retain title to this invention. Inquiries concerning rights for its commercial use should be addressed to:*

*Innovative Technology Assets Management*
*JPL*
*Mail Stop 202-233*
*4800 Oak Grove Drive*
*Pasadena, CA 91109-8099*
*E-mail: iaoffice@jpl.nasa.gov*
*Refer to NPO-46845, volume and number of this* NASA Tech Briefs *issue, and the page number.*

# High-Temperature Solid Lubricant Coating

*John H. Glenn Research Center, Cleveland, Ohio*

NASA PS400 is a solid lubricant coating invented for high-temperature tribological applications. This plasma-sprayed coating is a variant of the previously patented PS304 coating, and has been formulated to provide higher density, smoother surface finish, and better dimensional stability.

This innovation is a new composite material that provides a means to reduce friction and wear in mechanical compo-

nents. PS400 is a blend of a nickel-molybdenum binder, chrome oxide hardener, silver lubricant, and barium fluoride/calcium fluoride eutectic lubricant that can either be sprayed or deposited by other means, such as powder metallurgy. The resulting composite material is then finished by grinding and polishing to produce a smooth, self-lubricating surface.

*This work was done by Christopher Della-Corte and Brian J. Edmonds of Glenn Research Center. Further information is contained in a TSP (see page 1).Inquiries concerning rights for the commercial use of this invention should be addressed to NASA Glenn Research Center, Innovative Partnerships Office, Attn: Steven Fedor, Mail Stop 4–8, 21000 Brookpark Road, Cleveland, Ohio 44135. Refer to LEW-18561-1.*

## Mechanism for Particle Transport and Size Sorting via Low-Frequency Vibrations

### This technology would be useful for applications requiring sample handling.

*NASA's Jet Propulsion Laboratory, Pasadena, California*

There is a need for effective sample handling tools to deliver and sort particles for analytical instruments that are planned for use in future NASA missions. Specifically, a need exists for a compact mechanism that allows transporting and sieving particle sizes of powdered cuttings and soil grains that may be acquired by sampling tools such as a robotic scoop or drill. The required tool needs to be low mass and compact to operate from such platforms as a lander or rover. This technology also would be applicable to sample handling when transporting samples to analyzers and sorting particles by size.

A metal bar or plate with a linear array of asymmetric grooves has been designed to be shaken at low frequency by a voice coil, or linear actuator, mechanism which induces the particles to jump from one groove to the next. Larger particles with diameters greater than the groove depth were shown to move quicker, while particles with a diameter that is less than the groove depth were found to move slower, thus creating a sorting by size. Using this asymmetry in particle motion with particle size, it is shown that both the movement of unconsolidated particles along the slide provided both transportation and sorting mechanisms.

The initial motion of the plate was created by a rotary motor linked to create symmetric vibrations. The figure shows a graphic illustration of this system. The rotary motion can be used to sample unconsolidated material from a platform. A ro-
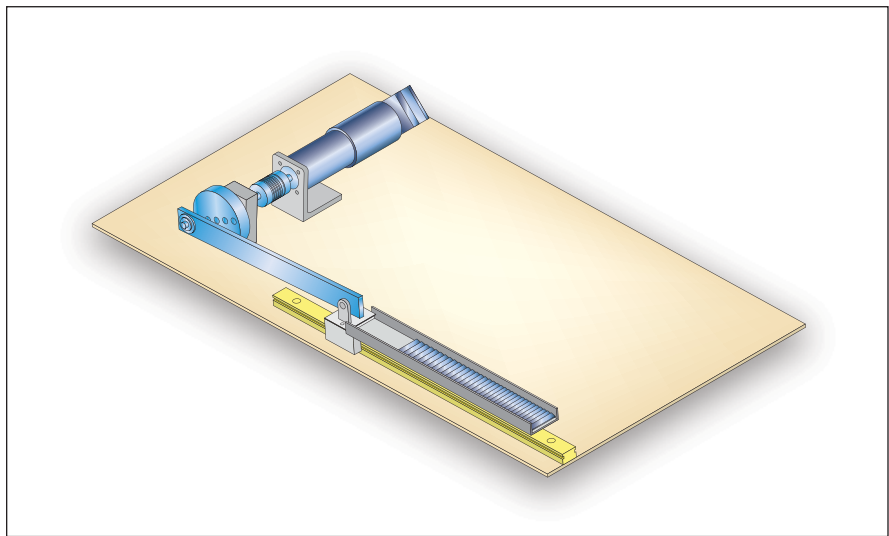


A **Schematic View of the System** using a rotary motor and a slide with asymmetric grooves.

tary motor causes linear oscillatory motion in the rod through a linkage, and causes particles in the grooves to move to higher-level grooves by being thrown from a lower groove. The linear actuation also could be developed with a voice coil actuator or any other linear motor. The use of asymmetric teeth increases the likelihood of a forward transfer of particles, and in each jump, the particles climb the toothlike steps. Introducing elliptical oscillations increases the efficiency of transfer by giving the sample movement vector normal to the slide axis.

An option to this design includes sieves to allow gauging of particle di-

mension. A distribution of particles is transported to the end of the groove rod. When particles enter a sieve with smaller holes, the excitation shakes them through the sieve. The excitation frequency is then increased, and the differentiated sample is then moved to the next larger size sieve where the process is repeated until all particles are sieved.

*This work was done by Stewart Sherrit, James S. Scott, Yoseph Bar-Cohen, Mircea Badescu, and Xiaoqi Bao of Caltech for NASA's Jet Propulsion Laboratory. Further information is contained in a TSP (see page 1). NPO-46334*

## Compact, Lightweight Electromagnetic Pump for Liquid Metal

### Overlapping thermal and magnetic issues are considered in this design increase efficiency.

*Marshall Space Flight Center, Alabama*

A proposed direct-current electromagnetic pump for circulating a molten alkali metal alloy would be smaller and lighter and would demand less input power, relative to currently available

pumps of this type. (Molten alkali metals are used as heat-transfer fluids in high-temperature stages of some nuclear reactors.) The principle of operation of this or any such pump involves exploita-

tion of the electrical conductivity of the molten metal: An electric current is made to pass through the liquid metal along an axis perpendicular to the longitudinal axis of the flow channel, and a
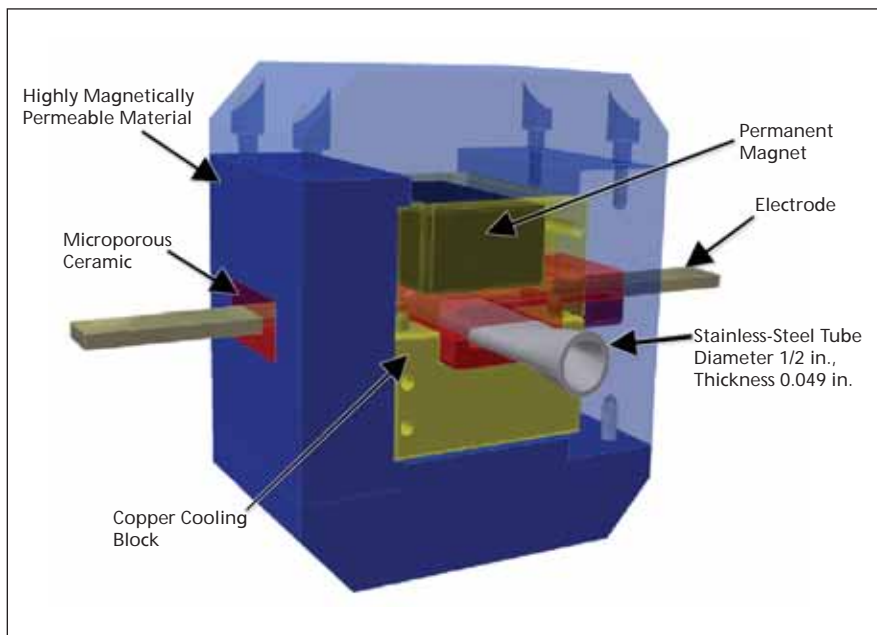
This **Direct-Current Electromagnetic Pump** is designed to develop a pressure of 5 psi (34 kPa) and a mass flow rate of 56 g/s when driven by an input current between 50 and 100 ADC (corresponding to an input potential of about 1 VDC). The pumped fluid would be a sodium-potassium eutectic at a temperature of about 650 °C.

magnetic field perpendicular to both the longitudinal axis and the electric current is superimposed on the flow-channel region containing the electric current. The interaction between the electric current and the magnetic field produces the pumping force along the longitudinal axis. The advantages of the proposed pump over other such pumps would accrue from design features that address overlapping thermal and magnetic issues.

Under the anticipated operating conditions, the molten alkali metal — a eutectic mixture of sodium and potassium — would be heated to a temperature of about 650 °C. To maximize the effectiveness of the pump while minimizing the electric current (and thus the power) needed for pumping at a given

rate, it is necessary to maximize the magnetic field across the flow channel. In order to do this, it would be desirable to use rare-earth (specifically, neodymium or samarium-cobalt) permanent magnets to apply the magnetic field and to place the magnets as close as possible to the flow channel. Because such magnets become demagnetized at temperatures around 130 or 350 °C, respectively, it becomes necessary to protect them against conduction and radiation of heat from the flow channel. In some other pumps of this type, the thermal-protection problem is solved by placing the magnets farther from the channel and then increasing the electric current needed to obtain the required pumping capacity. In still other pumps of this type, massive amounts of

convection cooling are used to prevent overheating of the magnets.

In the proposed pump, the liquid metal flow channel would be defined by a round stainless-steel tube that would be flattened to a nearly rectangular cross section in the region where the magnets were to be placed (see figure). Two permanent magnets would be placed on opposing sides of the channel, separated from the flat tube faces by thermal-insulation material consisting of a microporous ceramic having extremely low thermal conductivity. To remove the small amount of heat conducted through the ceramic, copper blocks housing the magnets are connected to a water-circulation cooling system. These blocks would be in direct thermal contact with each magnet, providing an isothermal heat sink to maintain the temperature below a required level. To maximize the magnetic flux density in the channel, the part of the magnetic circuit outside the channel would be completed with ferromagnetic material having a magnetic permeability and a magnetic-saturation threshold greater than those of simple iron.

Thick electrodes would conduct the applied electric current to the tube walls, and the current would be conducted through the tube walls to the liquid metal in the channel. A portion of the current would be conducted around the channel through the tube walls; this portion would not be available for generating pumping force. Hence, unavoidably, some power would be lost in heating of the tube walls.

# ✿ Progress in Development of the Axel Rovers
## Robots like these could be used to search for victims of disasters.

*NASA's Jet Propulsion Laboratory, Pasadena, California*

Progress has been made in the development of a family of robotic land vehicles having modular and minimalist design features chosen to impart a combination of robustness, reliability, and versatility. These vehicles at earlier stages of development were described in two previous *NASA Tech Briefs* arti-

cles: "Reconfigurable Exploratory Robotic Vehicles" (NPO-20944), Vol. 25, No. 7 (July 2001), page 56; and "More About Reconfigurable Exploratory Robotic Vehicles" (NPO-30890), Vol. 33, No. 8 (August 2009), page 40. Conceived for use in exploration of the surfaces of Mars and other remote

planets, these vehicles could also be adapted to terrestrial applications, including exploration of volcanic craters or other hostile terrain, military reconnaissance, inspection of hazardous sites, and searching for victims of earthquakes, landslides, avalanches, or mining accidents. In addition, simpli-

Figure 1. A **Prototype Axel Rover** can operate in a free or tethered configuration. Testing of this version is complicated by a need to properly wrap the power cable around the axle housing. It has been proposed to eliminate the power cable and install rechargeable batteries in a future version.
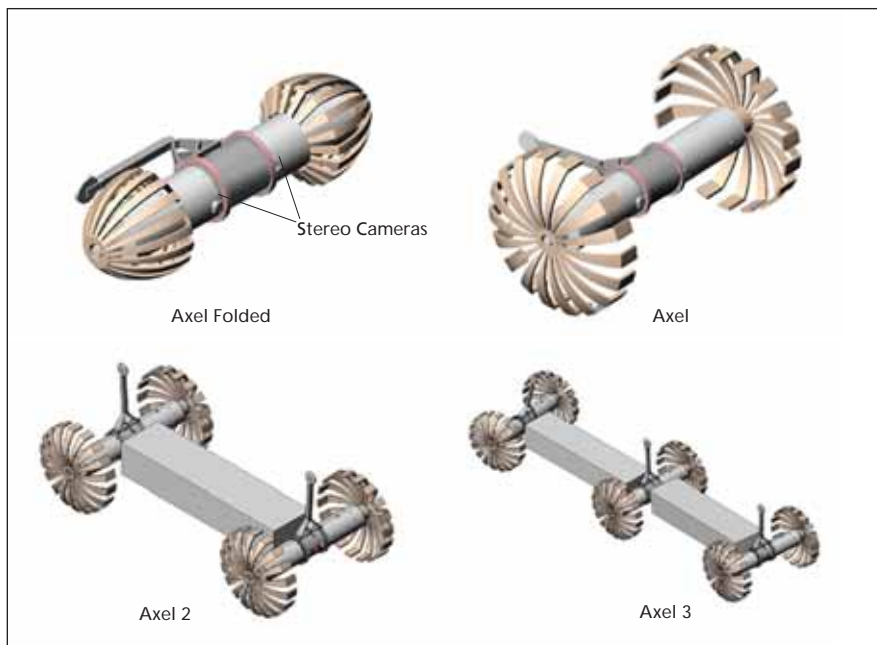


Figure 2. **Extended Axel Configurations** show design versatility.

fied versions of these vehicles might be marketable as toys.

The most basic module in this family of reconfigurable robots is the Axel rover, which has a cylindrical body with two main wheels and a trailing link. Inside its body are three motors and associated mechanisms for driving the two wheels and for rotating the link 360º around its symmetrical body. The actuated link serves several purposes:

• It is used as a lever arm to react to the wheels thrust to move Axel in multiple directions.
• It is used to rotate the Axel housing in order to tilt, to the desired angle, any sensors and instruments mounted on or in the Axel housing.
• It provides an alternative mobility mode, which is primarily used in its tethered configuration. Turning the link into the ground in lieu of driving

the wheels causes the Axel housing and wheels to roll as a unit and thereby leads to a tumbling motion along the ground. With a tether mounted around Axel's cylindrical body, the link serves as a winch mechanism to reel and unreel the tether raising and lowering Axel over steep and vertical surfaces (Figure 1).

Sensors, computation, and communication modules are also housed inside Axel's body. A pair of stereo vision cameras provides three-dimensional view for autonomous navigation and avoiding obstacles. Inertial sensors determine the tilt of the robot and are used for estimating its motion. In a fully developed version, power would be supplied by rechargeable batteries aboard Axel; at the time of reporting the information for this article, power was supplied from an external source via a cable.

In and of itself, the Axel rover is fully capable of traversing and sampling terrains on planetary surfaces. By use of only the two main wheel actuators and the caster link actuator, Axel can be made to follow an arbitrary path, turn in place, and operate upside-down or right-side-up. If operated in a tethered configuration, as shown in Figure 1, it can be made to move down and up a steep crater wall, descend from an overhang to a cave, and ascend from the cave back to the overhang, all by use of the same three actuators. Such tethered operation could be useful in searching for accident victims or missing persons in mines, caves, and rubble piles. Running the tether through the caster link enhances the stability of Axel and provides a restoring force that keeps the link off the ground for the most part during operation on a steep slope.

In its extended configuration, two Axel modules can dock to either side of a payload module to form the four wheeled Axel2 rover (Figure 2). Additional payload and Axel modules can dock to either side of the Axel2 to form the Axel3 rover, extending its payload capacity and its mobility capabilities.

# Compact, Lightweight Servo-Controllable Brakes

*Lyndon B. Johnson Space Center, Houston, Texas*

Compact, lightweight servo-controllable brakes capable of high torques are being developed for incorporation into robot joints. A brake of this type is based partly on the capstan effect of tension elements, which is described by the well-known equation

$$T_h / T_l = e^{\mu\beta},$$

where $T_h$ is the higher tension at one end and $T_l$ is the lower tension at the other end of a rope, belt, chain, or other tension element that is wrapped around a capstan so as not to slip; $\beta$ is the total wrap angle in radians; and $\mu$ is the coefficient of friction between the capstan and the tension element. For example, a tension-multiplication factor of the order of $10^6$ can be achieved by wrapping several turns of steel wire around a steel capstan. Heretofore, the capstan effect has been exploited in wound-spring clutches that operate in an on-or-off fashion. In a brake of the type under development, a controllable intermediate state of torque is reached through on/off switching at a high frequency.

This work was done by Christopher S. Lovchik of Johnson Space Center, William Townsend and Jeffrey Guertin of Barrett Technology, Inc., and Yoky Matsuoka of Carnegie Mellon University. For further information, contact the JSC Innovation Partnerships Office at (281) 483-3809.
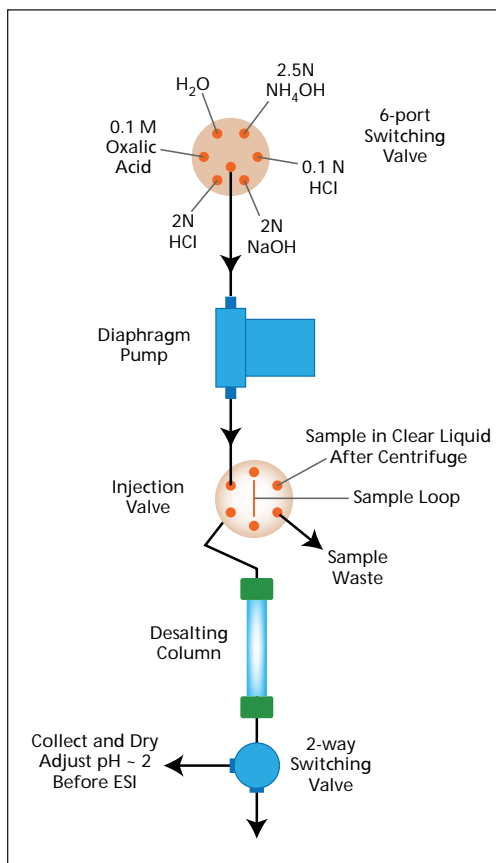
# Automated Desalting Apparatus

**By purifying field samples, this technology can be used for monitoring of water quality for applications in chemical, manufacturing, and farming industries.**

*NASA's Jet Propulsion Laboratory, Pasadena, California*

Because salt and metals can mask the signature of a variety of organic molecules (like amino acids) in any given sample, an automated system to purify complex field samples has been created for the analytical techniques of electrospray ionization/mass spectroscopy (ESI/MS), capillary electrophoresis (CE), and biological assays where unique identification requires at least some processing of complex samples. This development allows for automated sample preparation in the laboratory and analysis of complex samples in the field with multiple types of analytical instruments.

Rather than using tedious, exacting protocols for desalting samples by hand, this innovation, called the Automated Sample Processing System (ASPS), takes analytes that have been extracted through high-temperature solvent extraction and introduces them into the desalting column. After 20 minutes, the eluent is produced. This clear liquid can then be directly analyzed by the techniques listed above. The current apparatus including the computer and power supplies is sturdy, has an approximate mass of 10 kg, and a volume of about 20×20×20 cm, and is undergoing further miniaturization.



The **Automated Desalting Apparatus** includes two mutli-port valves, a diaphragm valve, and an ion exchange column. Six different solvents are required to both process the sample and condition the column before and after processing.

This system currently targets amino acids. For these molecules, a slurry of 1 g cation exchange resin in deionized water is packed into a column of the apparatus. Initial generation of the resin is done by flowing sequentially 2–3 bed volumes of 2N NaOH and 2N HCl (1 mL each) to rinse the resin, followed by ≈5 mL of deionized water. This makes the pH of the resin near neutral, and eliminates cross sample contamination. Afterward, 2–3 mL of extracted sample is then loaded into the column onto the top of the resin bed. Because the column is packed tightly, the sample can be applied without disturbing the resin bed. This is a vital step needed to ensure that the analytes adhere to the resin.

After the sample is drained, oxalic acid (1 mL, pH 1.6-1.8, adjusted with $NH_4OH$) is pumped into the column. Oxalic acid works as a chelating reagent to bring out metal ions, such as calcium and iron, which would otherwise interfere with amino acid analysis. After oxalic acid, 1 mL 0.01 N HCl and 1 mL deionized water is used to sequentially rinse the resin. Finally, the amino acids attached to the resin, and the analytes are eluted using 2.5 M $NH_4OH$ (1 mL), and the $NH_4OH$ eluent is collected in a vial for analysis.

All of these steps are controlled by Lab-VIEW software, which controls 7-way, two 2-way valves, as well as a peristaltic pump. Solvents are all attached to the 7-way valve and are introduced by the peristaltic pump at flow rates on the order of 1-5 μL/min.

# ❇ Durable Tactile Glove for Human or Robot Hand

*Lyndon B. Johnson Space Center, Houston, Texas*

A glove containing force sensors has been built as a prototype of tactile sensor arrays to be worn on human hands and anthropomorphic robot hands. Whereas the force sensors of a prior force-sensing glove are mounted on the outside, the force sensors of this glove are mounted inside, in protective pockets; as a result of this and other design features, the present glove is more durable. The sensors, which cost only $3 apiece (2002), produce analog force readings in the range of 0 to 5 lb (0 to 22 N) at numerous locations across the hand.

To minimize false readings due to internal glove motions and/or tight fit of the glove on the hand, the pockets are constructed as recesses within modular foam inserts that are sewn into the glove. High-friction material provides good gripping surfaces for finger and palm contact areas. Textile stiffeners on the backsides of the sensors prevent deformation of the foam during motion. To ensure that forces are directed into the sensors and not channeled through the relatively stiff gripping-surface material, stiff plastic beads are sewn in place between the sensors and the outer glove fabric.

# ❇ Robotic Arm Manipulator Using Active Control for Sample Acquisition and Transfer, and Passive Mode for Surface Compliance

*NASA's Jet Propulsion Laboratory, Pasadena, California*

A robotic arm that consists of three joints with four degrees of freedom (DOF) has been developed. It can carry an end-effector to acquire and transfer samples by using active control and comply with surface topology in a passive mode during a brief surface contact. The three joints are arranged in such a way that one joint of two DOFs is located at the shoulder, one joint of one DOF is located at the elbow, and one joint of one DOF is located at the wrist. Operationally, three DOFs are moved in the same plane, and the remaining one on the shoulder is moved perpendicular to the other three for better compliance with ground surface and more flexibility of sample handling. Three out of four joints are backdriveable, making the mechanism less complex and more cost effective.

Having joints of a robotic arm accomplish two different tasks is a new concept. The preliminary engineering shows this concept is workable with proper selection of actuators.

# Suppressing Loss of Ions in an Atomic Clock

**Ion traps are excited at two different frequencies.**

*NASA's Jet Propulsion Laboratory, Pasadena, California*

An improvement has been made in the design of a compact, highly stable mercury-ion clock to suppress a loss of ions as they are transferred between the quadrupole and higher multipole ion traps. Such clocks are being developed for use aboard spacecraft for navigation and planetary radio science. The modification is also applicable to ion clocks operating on Earth: indeed, the success of the modification has been demonstrated in construction and operation of a terrestrial breadboard prototype of the compact, highly stable mercury-ion clock.

Selected aspects of the breadboard prototype at different stages of development were described in previous *NASA Tech Briefs* articles. The following background information is reviewed from previous articles: In this clock as in some prior ion clocks, mercury ions are shuttled between two ion traps, one a 16-pole linear radio-frequency trap, while the other is a quadrupole radio-frequency trap. In the quadrupole trap, ions are tightly confined and optical state selection from a $^{202}$Hg lamp is carried out. In the 16-pole trap, the ions are more loosely confined and atomic transitions are interrogated by use of a microwave beam at approximately 40.507

GHz. The trapping of ions effectively eliminates the frequency pulling that would otherwise be caused by collisions between clock atoms and the wall of a gas cell. The shuttling of the ions between the two traps enables separation of the state-selection process from the clock microwave-resonance process, so that each of these processes can be optimized independently of the other. This is similar to the operation of an atomic beam clock, except that with ions the "beam" can be halted and reversed as ions are shuttled back and forth between the two traps.

When the two traps are driven at the same radio frequency, the strength of confinement can be reduced near the junction between the two traps, depending upon the relative phase of the RF voltage used to operate each of the two traps, and can cause loss of ions during each transit between the traps and thereby cause loss of the 40.507-GHz ion-clock resonance signal.

The essence of the modification is to drive the two traps at different frequencies — typically between 1.5 and 2 MHz for the quadrupole trap and a frequency a few hundred kHz higher for the 16-pole trap. A frequency difference of a

few hundred kHz ensures that the ion motion caused by the trapping electric fields is small relative to the diameter of the traps. Unlike in the case in which both traps are driven at the same frequency, the trapping electric fields near the junction are not zero at all times; instead, the regions of low electric field near the junction open and close at the difference frequency. An additional benefit of making the 16-pole trap operate at higher frequency is that the strength or depth of the multipole trap can be increased independent of the quadrupole ion trap.

# Simplified Vicarious Radiometric Calibration

**At-sensor radiance is estimated more directly than in prior methods.**

*Stennis Space Center, Mississippi*

A measurement-based radiance estimation approach for vicarious radiometric calibration of spaceborne multispectral remote sensing systems has been developed. This simplified process eliminates the use of radiative transfer codes and reduces the number of atmospheric assumptions required to perform sensor calibrations. Like prior approaches, the simplified method involves the collection of ground truth data coincident with the overpass of the remote sensing system being calibrated,

but this approach differs from the prior techniques in both the nature of the data collected and the manner in which the data are processed.

In traditional vicarious radiometric calibration, ground truth data are gathered using ground-viewing spectroradiometers and one or more sun photometer(s), among other instruments, located at a ground target area. The measured data from the ground-based instruments are used in radiative transfer models to estimate the top-of-atmos-

phere (TOA) target radiances at the time of satellite overpass. These TOA radiances are compared with the satellite sensor readings to radiometrically calibrate the sensor.

Traditional vicarious radiometric calibration methods require that an atmospheric model be defined such that the ground-based observations of solar transmission and diffuse-to-global ratios are in close agreement with the radiative transfer code estimation of these parameters. This process is labor-intensive and

complex, and can be prone to errors. The errors can be compounded because of approximations in the model and inaccurate assumptions about the radiative coupling between the atmosphere and the terrain. The errors can increase the uncertainty of the TOA radiance estimates used to perform the radiometric calibration.

In comparison, the simplified approach does not use atmospheric radiative transfer models and involves fewer assumptions concerning the radiative transfer properties of the atmosphere. This new technique uses two neighboring uniform ground target areas having different reflectance values. The target areas can be natural or artificial and must be large enough to minimize adjacent-pixel contamination effects. The radiative coupling between the atmosphere and the terrain needs to be approximately the same for the two targets. This condition can be met for relatively uniform backgrounds when the distance between the targets is within a few hundred meters.

For each target area, the radiance leaving the ground in the direction of the satellite is measured with a radiometrically calibrated spectroradiometer. Using the radiance measurements from the two targets, atmospheric adjacency and atmospheric scattering effects can be subtracted, thereby eliminating many assumptions about the atmosphere and the radiative interaction between the atmosphere and the terrain. In addition, the radiometrically calibrated spectroradiometer can be used with a known reflectance target to estimate atmospheric transmission and diffuse-to-global ratios without the need for ancillary sun photometers.

Several comparisons between the simplified method and traditional techniques were found to agree within a few percent. Hence, the simplified method reduces the overall complexity of performing vicarious calibrations and can serve as a method for validating traditional radiative transfer models.

# Phase-Conjugate Receiver for Gaussian-State Quantum Illumination

## Active optical sensors have application in military surveillance.

*NASA's Jet Propulsion Laboratory, Pasadena, California*

An active optical sensor probes a region of free space that is engulfed in bright thermal noise to determine the presence (or absence) of a weakly reflecting target. The returned light (which is just thermal noise if no target is present, and thermal noise plus a weak reflection of the probe beam if a target is present) is measured and processed by a receiver and a decision is made on whether a target is present.

It has been shown that generating an entangled pair of photons (which is a highly nonclassical state of light), using one photon as the probe beam and storing the other photon for comparison to the returned light, has superior performance to the traditional classical-light (coherent-state) target detection sensors. An entangled-photon transmitter and optimal receiver combination can yield up to a factor of 4 (i.e., 6 dB) gain in the error-probability exponent over a coherent state transmitter and optimal receiver combination, in a highly lossy and noisy scenario (when both sensors have the same number of transmitted photons). However, the receiver that achieves this advantage is not known. One structured receiver can close half of the 6-dB gap (i.e., a 3-dB improvement). It is based on phase-conjugating the returned light, then performing dual-balanced difference detection with the stored half of the entangled-photon pair.

Active optical sensors are of tremendous value to NASA's missions. Although this work focuses on target detection, it can be extended to imaging (2D, 3D, hyperspectral, etc.) scenarios as well, where the image quality can be better than that offered by traditional active sensors. Although the current work is theoretical, NASA's future missions could benefit significantly from developing and demonstrating this capability.

This is an optical receiver design whose components are, in principle, all implementable. However, the work is currently entirely theoretical. It is necessary to:
1. Demonstrate a bench-top proof of the theoretical principle,
2. Create an operational prototype off-the-bench, and
3. Build a practical sensor that can fly in a mission.

# Improved Tracking of an Atomic-Clock Resonance Transition

## The resonance frequency is repeatedly estimated from sequences of three measurements.

*NASA's Jet Propulsion Laboratory, Pasadena, California*

An improved method of making an electronic oscillator track the frequency of an atomic-clock resonance transition is based on fitting a theoretical nonlinear curve to measurements at three oscillator frequencies within the operational frequency band of the transition (in other words, at three points within the resonance peak). In the measurement process, the frequency of a microwave oscillator is repeatedly set at various offsets from the nominal resonance
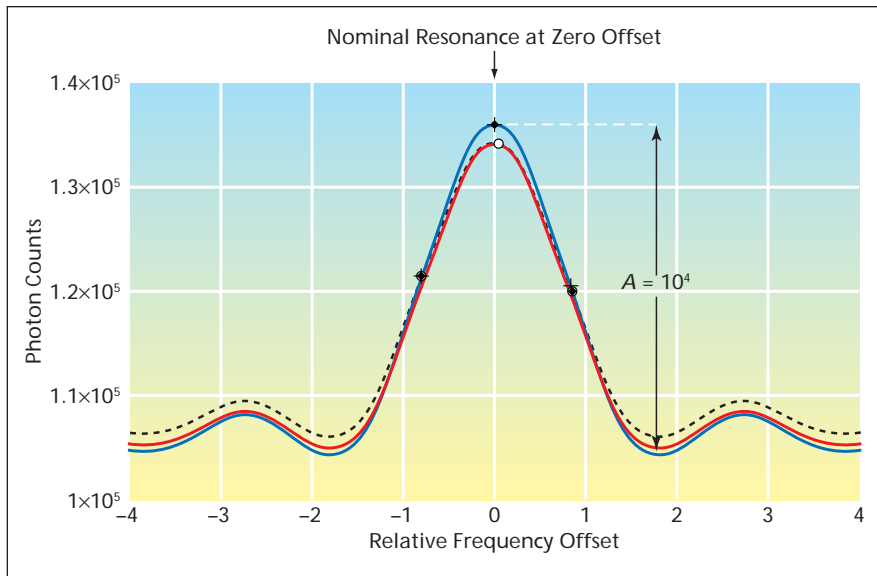
**These Three Plots** represent fits of the nonlinear curve to three sets of simulated measurements, each set comprising photon counts at relative frequency offsets ($y$ values) of 0 and ±0.761. The parameters of the simulated measurements were $B = 1.05 \times 10^5$ counts, $A = 3 \times 10^4$ counts, and signal-to-noise ratio ≈30.

frequency, the oscillator signal is applied in a square pulse of the oscillator signal having a suitable duration (typically, of the order of a second), and, for each pulse at each frequency offset, fluorescence photons of the transition in question are counted. As described below, the counts are used to determine a new nominal resonance frequency. Thereafter, offsets are determined with respect to the new resonance frequency. The process as described thus far is repeated so as to repeatedly adjust the oscillator to track the most recent estimate of the nominal resonance frequency.

The theoretical nonlinear curve is that of the Rabi equation for the shape of the resonance peak

$$P(y) = \frac{\sin^2\left(\frac{\pi}{2}\sqrt{1+y^2}\right)}{1+y^2}$$

where the dimensionless variable $y$ is related to the duration of the microwave pulse, $T$, and the frequency offset $\nu - \nu_0$ from the atomic absorption frequency, $\nu_0$, as follows: $y = 2T(\nu - \nu_0)$.

Assuming that the signal power has been optimized and that the photon count at a given measurement signal frequency includes a non-resonant background contribution plus a contribution attributable to the resonance, the basic measurement equation for the $i$th measurement is

$$C(i) = B + AP(y_1 - \varepsilon)$$

where $C(i)$ is the atomic fluorescence photon count, $A$ is atomic fluorescence, and $\varepsilon$ is an offset of the nominal resonance frequency from the actual resonance frequency. If measurements are made at three different oscillator frequency offsets ($y_1, y_2, y_3$), then one has

$$C(1) = B + AP(y_1 - \varepsilon)$$
$$C(2) = B + AP(y_2 - \varepsilon)$$
$$C(3) = B + AP(y_3 - \varepsilon)$$

Repeatedly, for the most recent such set of three measurements (see figure), this set of three equations is inverted to extract $B$, $A$, and $\varepsilon$ from the measurement values $C(1)$, $C(2)$, and $C(3)$. Because the solution obtained through inversion of the three equations separates the influences of background light, signal strength, and the offset of the resonance from the nominal resonance frequency, unlike in a prior method, drift in the power of the lamp used to excite the clock atoms to the upper level of the transition does not seem to effect frequency pulling (that is, it does not seem to force a change in the estimate of the resonance frequency).

# Measurement of the Length of an Optical Trap
## This technique aids in the assembly of MEMS devices.

*John H. Glenn Research Center, Cleveland, Ohio*

NASA Glenn has been involved in developing optical trapping and optical micromanipulation techniques in order to develop a tool that can be used to probe, characterize, and assemble nano and microscale materials to create microscale sensors for harsh flight environments. In order to be able to assemble a sensor or probe candidate sensor material, it is useful to know how far an optical trap can "reach"; that is, the distance beyond/below the stable trapping point through which an object will be drawn into the optical trap. Typically, to measure the distance over which an op-

tical trap would influence matter in a horizontal (perpendicular to beam propagation) direction, it was common to hold an object in one optical trap, place a second optical trap a known distance away, turn off the first optical trap, and note if the object was moved into the second trap when it was turned on. The disadvantage of this technique is that it only gives information of trap influence distance in horizontal ($x$–$y$) directions. No information about the distance of the influence of the trap is gained in the direction of propagation of the beam (the $z$ direction).

A method was developed to use a time-of-flight technique to determine the length along the propagation direction of an optical trap beam over which an object may be drawn into the optical trap. Test objects (polystyrene microspheres) were held in an optical trap in a water-filled sample chamber and raised to a pre-determined position near the top of the sample chamber. Next, the test objects were released by blocking the optical trap beam. The test objects were allowed to fall through the water for predetermined periods of time, at the end of which the trapping beam was unblocked. It was noted

whether or not the test object returned to the optical trap or continued to fall.

This determination of the length of an optical trap's influence by this manner assumes that the test object falls through the water in the sample chamber at terminal velocity for the duration of its fall, so that the distance of trap influence can be computed simply by: $d = V_T t$, where $d$ is the trap length (or distance of trap reach), $V_T$ is the terminal velocity of the test object, and $t$ is the time interval over which the object is allowed to fall. In order for this methodology to work, it must be established that the test object indeed falls through the water in the sam-

ple chamber at terminal velocity. This answers the question of how far below the trap point an object must be to be drawn into an optical trap in order to select and manipulate material for microscale assembly and characterization.

This methodology would make it possible for optical trapping to be incorporated into the assembly of MEMS (microelectromechanical systems) devices. In particular, adding pieces or connectors to MEMS devices that cannot be positioned via photolithography and vapor or film deposition techniques may be added to a MEMS device via placement by optical traps. In this case, it is impera-

tive to know how far beyond the stable trapping point in the direction of propagation of the beam an object should or must be to be trapped, and also the distance beyond the stable optical trapping point over which the propagating laser beam has no effect.

# Phase-Array Approach to Optical Whispering Gallery Modulators

*NASA's Jet Propulsion Laboratory, Pasadena, California*

This technology leverages the well-defined orbital number of a whispering gallery modulator (WGM) to expand the range of applications for such resonators. This property rigidly connects the phase variation of the field in this mode with the azimuthal angle between the coupling locations.

A WGM with orbital momentum $L$ has exactly $L$ instant nodes around the circumference of the WGM resonator supporting such a mode. Therefore, in two locations separated by the arc $\alpha$, the phase difference of such a field will be

equal to $\phi = \alpha L$. Coupling the field out of such locations, and into a balanced interferometer, once can observe a complete constructive or distractive interference (or have any situation in between) depending on the angle $\alpha$. Similarly, a mode $L + \Delta L$ will pick up the phase $\phi + \alpha \Delta L$.

In all applications of a WGM resonator as a modulator, the orbital numbers for the carrier and sidebands are different, and their differences $\Delta L$ are known (usually, but not necessarily, $\Delta L = 1$). Therefore, the choice of the angle $\alpha$, and of the interferometer arms differ-

ence, allows one to control the relative phase between different modes and to perform the conversion, separation, and filtering tasks necessary.

# Infrared Camera System for Visualization of IR-Absorbing Gas Leaks

## This system is applicable in HVAC, methane production plants, and oil refineries.

*John F. Kennedy Space Center, Florida*

Leak detection and location remain a common problem in NASA and industry, where gas leaks can create hazardous conditions if not quickly detected and corrected. In order to help rectify this problem, this design equips an infrared (IR) camera with the means to make gas leaks of IR-absorbing gases more visible for leak detection and location.

By comparing the output of two IR cameras (or two pictures from the same camera under essentially identical conditions and very closely spaced in time) on a pixel-by-pixel basis, one can cancel out all but the desired varia-

tions that correspond to the IR absorption of the gas of interest. This can be simply done by absorbing the IR lines that correspond to the gas of interest from the radiation received by one of the cameras by the intervention of a filter that removes the particular wavelength of interest from the "reference" picture. This can be done most sensitively with a gas filter (filled with the gas of interest) placed in front of the IR detector array, or (less sensitively) by use of a suitable line filter in the same location.

This arrangement would then be balanced against the unfiltered "measure-

ment" picture, which will have variations from IR absorption from the gas of interest. By suitable processing of the signals from each pixel in the two IR pictures, the user can display only the differences in the signals. Either a difference or a ratio output of the two signals is feasible. From a gas concentration viewpoint, the ratio could be processed to show the column depth of the gas leak. If a variation in the background IR light intensity is present in the field of view, then large changes in the difference signal will occur for the same gas column concentration between the background and the camera. By ratioing the outputs, the
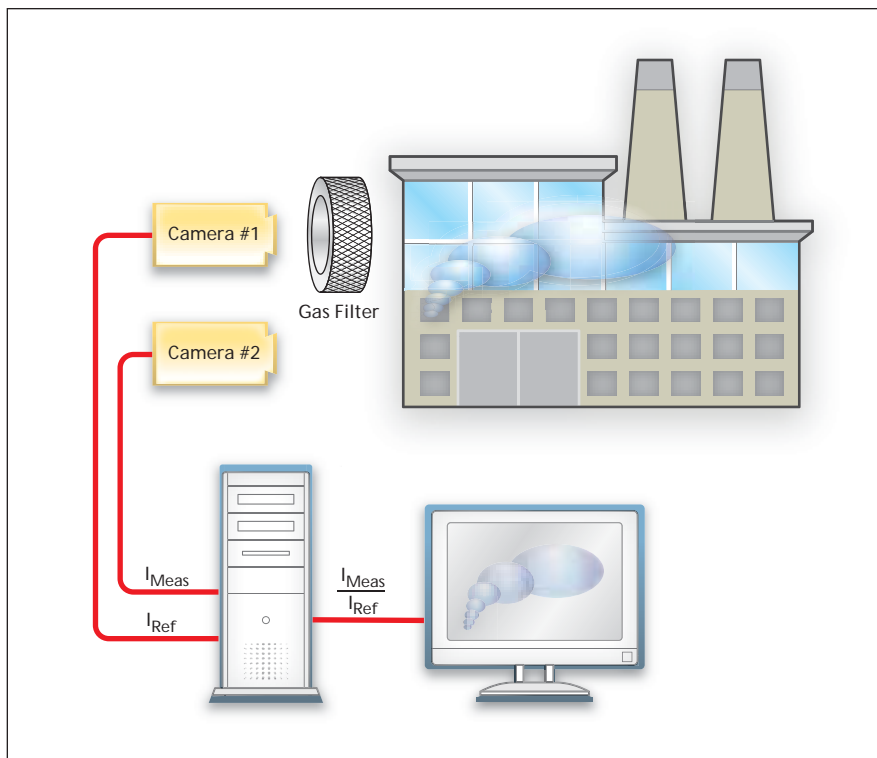
The **Two-Camera Version of the Infrared Camera System** features two cameras with essentially the same view and time.

same signal ratio is obtained for both high- and low-background signals, even though the low-signal areas may have greater noise content due to their smaller signal strength. Thus, one embodiment would use a ratioed output signal to better represent the gas column concentration.

An alternative approach uses a simpler multiplication of the filtered signal to make the filtered signal equal to the unfiltered signal at most locations, followed by a subtraction to remove all but the wavelength-specific absorption in the unfiltered sample. This signal processing can also reveal the net difference signal representing the leaking gas absorption, and allow rapid leak location, but signal intensity would not relate solely to gas absorption, as raw signal intensity would also affect the displayed signal.

A second design choice is whether to use one camera with two images closely spaced in time, or two cameras with essentially the same view and time. The figure shows the two-camera version. This choice involves many tradeoffs that are not apparent until some detailed testing is done. In short, the tradeoffs involve the temporal changes in the field picture versus the pixel sensitivity curves and frame alignment differences with two cameras, and which system would lead to the smaller variations from the uncontrolled variables.

# Submonolayer Quantum Dot Infrared Photodetector

*NASA's Jet Propulsion Laboratory, Pasadena, California*

A method has been developed for inserting submonolayer (SML) quantum dots (QDs) or SML QD stacks, instead of conventional Stranski-Krastanov (S-K) QDs, into the active region of intersubband photodetectors. A typical configuration would be InAs SML QDs embedded in thin layers of GaAs, surrounded by AlGaAs barriers. Here, the GaAs and the AlGaAs have nearly the same lattice constant, while InAs has a larger lattice constant.

In QD infrared photodetector, the important quantization directions are in the plane perpendicular to the normal incidence radiation. In-plane quantization is what enables the absorption of normal incidence radiation. The height of the S-K QD controls the positions of the quantized energy levels, but is not critically important to the desired normal incidence absorption properties. The SML QD or SML QD stack configurations give more control of the structure grown, retains normal incidence absorption properties, and decreases the strain build-up to allow thicker active layers for higher quantum efficiency.

# Mode Tracker for Mode-Hop-Free Operation of a Laser

*Lyndon B. Johnson Space Center, Houston, Texas*

A mode-tracking system that includes a mode-controlling subsystem has been incorporated into an external-cavity (EC) quantum cascade laser that operates in a mid-infrared wavelength range.

The mode-tracking system makes it possible to perform mode-hop-free wavelength scans, as needed for high-resolution spectroscopy and detection of trace gases. The laser includes a gain chip, a beam-collimating lens, and a diffraction grating. The grating is mounted on a platform, the position of which can be varied to effect independent control of the EC length and the grating angle.

The position actuators include a piezo-electric stage for translation control and a motorized stage for coarse rotation control equipped with a piezoelectric actuator for fine rotation control. Together, these actuators enable control of the EC length over a range of about 90 μm with a resolution of 0.9 nm, and control of the grating angle over a coarse-tuning range of ±6.3° and a fine-tuning range of ±520 μrad with a resolution of 10 nrad. A mirror mounted on the platform with the grating assures always the same direction of the output laser beam.

*This work was done by Gerard Wysocki, Frank K. Tittel, and Robert F. Curl of Rice University for Johnson Space Center.*

*In accordance with Public Law 96-517, the contractor has elected to retain title to this invention. Inquiries concerning rights for its commercial use should be addressed to:*

*Rice University*
*Office of Technology Transfer*
*MS-705*
*6100 Main Street*
*Houston Texas 77005-1892*
*Phone No: (713)-348-6188*
*E-mail: techtran@rice.edu*
*Refer to MSC-24088-1, volume and number of this* NASA Tech Briefs *issue, and the page number.*

# Fiber-Optic Continuous Liquid Sensor for Cryogenic Propellant Gauging

## Either water or liquid nitrogen levels can be measured within 1-mm spatial resolution and 1°C up to a distance of 70 m from the optical interrogation unit.

*John H. Glenn Research Center, Cleveland, Ohio*

An innovative fiber-optic sensor has been developed for low-thrust-level settled mass gauging with measurement uncertainty <0.5 percent over cryogenic propellant tank fill levels from 2 to 98 percent. The proposed sensor uses a single optical fiber to measure liquid level and liquid distribution of cryogenic propellants. Every point of the sensing fiber is a "point sensor" that not only distinguishes liquid and vapor, but also measures temperature. This sensor is able to determine the physical location of each "point sensor" with 1-mm spatial resolution. Acting as a continuous array of numerous liquid/vapor point sensors, the truly distributed optical sensing fiber can be installed in a propellant tank in the same manner as silicon diode point sensor stripes using only a single feed-through to connect to an optical signal interrogation unit outside the tank.

Either water or liquid nitrogen levels can be measured within 1-mm spatial resolution up to a distance of 70 meters from the optical interrogation unit. This liquid-level sensing technique was also compared to the pressure gauge measurement technique in water and liquid nitrogen contained in a vertical copper pipe with a reasonable degree of accuracy. It has been demonstrated that the sensor can measure liquid levels in multiple containers containing water or liquid nitrogen with one signal interrogation unit. The liquid levels measured by the multiple fiber sensors were consistent with those virtually measured by a ruler.

The sensing performance of various optical fibers has been measured, and has demonstrated that they can survive after immersion at cryogenic temperatures. The fiber strength in liquid nitrogen has also been measured. Multiple water level tests were also conducted under various actual and theoretical vibration conditions, and demonstrated that the signal-to-noise ratio under these vibration conditions, insofar as it affects measurement accuracy, is manageable and robust enough for a wide variety of spacecraft applications. A simple solution has been developed to absorb optical energy at the termination of the optical sensor, thereby avoiding any feedback to the optical interrogation unit.

*This work was done by Wei Xu of Broadband Photonics for Glenn Research Center. Further information is contained in a TSP (see page 1).*

*Inquiries concerning rights for the commercial use of this invention should be addressed to NASA Glenn Research Center, Innovative Partnerships Office, Attn: Steve Fedor, Mail Stop 4–8, 21000 Brookpark Road, Cleveland, Ohio 44135. Refer to LEW-18505-1.*

# Ionization-Assisted Getter Pumping for Ultra-Stable Trapped Ion Frequency Standards

*NASA's Jet Propulsion Laboratory, Pasadena, California*

A method eliminates (or recovers from) residual methane buildup in getter-pumped atomic frequency standard systems by applying ionizing assistance. Ultra-high stability trapped ion frequency standards for applications requiring very high reliability, and/or low power and mass (both for ground-based and space-based platforms) benefit from using sealed vacuum systems. These systems require careful material selection and system processing (cleaning and high-temperature bake-out). Even under the most careful preparation, residual hydrogen outgassing from vacuum chamber walls typically limits the base pressure.

Non-evaporable getter pumps (NEGs) provide a convenient pumping option for sealed systems because of low mass and volume, and no power once activated. However, NEGs do not pump inert gases, methane, and some other hydrocarbon gases. For ultra-high vacuum applications, methane can become the single largest un-pumped component. Methane collisions with trapped ions (such as $^{199}Hg^+$) used for frequency standard applications can produce de-coher-

ence and a very large frequency shift, both significant limitations to high-performance frequency standard operation. Therefore, any methane presence, or buildup in the vacuum system over time, can negate the benefit of getter pumping and degrade frequency standard performance.

It is well known that the presence of a hot surface at or above a particular temperature threshold in a vacuum chamber can "crack" residual methane ($CH_4$ or other similar hydrocarbons), dissociating it into C and $H_2$. Each of these can be readily removed by a getter pump. This cracking process can occur when methane molecules interact with the hot tungsten filament of an ion gauge (ionization-assisted gettering). In this case, methane molecules are dissociated either via direct interaction with the hot filament or via electron impact.

Thus an ion gauge in conjunction with a NEG can be used to provide a low-mass, low-power method for avoiding the deleterious effects of methane buildup in high-performance frequency standard vacuum systems.

## Physical Invariants of Intelligence

**Current research involves a quantumlike aspect of mental-to-motor feedback.**

*NASA's Jet Propulsion Laboratory, Pasadena, California*

A program of research is dedicated to development of a mathematical formalism that could provide, among other things, means by which living systems could be distinguished from non-living ones. A major issue that arises in this research is the following question: What invariants of mathematical models of the physics of systems are (1) characteristic of the behaviors of intelligent living systems and (2) do not depend on specific features of material compositions heretofore considered to be characteristic of life?

This research at earlier stages has been reported, albeit from different perspectives, in numerous previous *NASA Tech Briefs* articles. To recapitulate: One of the main underlying ideas is to extend the application of physical first principles to the behaviors of living systems. Mathematical models of motor dynamics are used to simulate the observable physical behaviors of systems or objects of interest, and models of mental dynamics are used to represent the evolution of the corresponding knowledge bases. For a given system, the knowledge base is modeled in the form of probability distributions and the mental dynamics is represented by models of the evolution of the probability densities or, equivalently, models of flows of information.

At the time of reporting the information for this article, the focus of this research was upon the following aspects of the formalism: Intelligence is considered to be a means by which a living system preserves itself and improves its ability to survive and is further considered to manifest itself in feedback from the mental dynamics to the motor dynamics. Because of the feedback from the mental dynamics, the motor dynamics attains quantumlike properties: The trajectory of the physical aspect of the system in the space of dynamical variables splits into a family of different trajectories, and each of those trajectories can be chosen with a probability prescribed by the mental dynamics.

From a slightly different perspective, the mechanism of decision-making is feedback from the mental dynamics to the motor dynamics, and this mechanism provides a quantumlike collapse of a random motion into an appropriate deterministic state, such that entropy undergoes a pronounced decrease. The existence of this mechanism is considered to be an invariant of intelligent behavior of living systems, regardless of the origins and material compositions of the systems.

*This work was done by Michail Zak of Caltech for NASA's Jet Propulsion Laboratory. For more information, contact iaoffice@jpl.nasa.gov. NPO-46085*

## Rocket-Plume Spectroscopy Simulation for Hydrocarbon-Fueled Rocket Engines

**Enhanced simulation includes code for new electronic bands in the 300-to-850-nm spectral bands.**

*Stennis Space Center, Mississippi*

The UV-Vis spectroscopic system for plume diagnostics monitors rocket engine health by using several analytical tools developed at Stennis Space Center (SSC), including the rocket plume spectroscopy simulation code (RPSSC), to identify and quantify the alloys from the metallic elements observed in engine plumes. Because the hydrocarbon-fueled rocket engine is likely to contain $C_2$, CO, CH, CN, and NO in addition to OH and $H_2O$, the relevant electronic bands of these molecules in the spectral range of 300 to 850 nm in the RPSSC have been included.

SSC incorporated several enhancements and modifications to the original line-by-line spectral simulation computer program implemented for plume spectral data analysis and quantification in 1994. These changes made the program applicable to the Space Shuttle Main Engine (SSME) and the Diagnostic Testbed Facility Thruster (DTFT) exhaust plume spectral data. Modifications included updating the molecular and spectral parameters for OH, adding spectral parameter input files optimized for the 10 elements of interest in the spectral range from 320 to 430 nm and linking the output to graphing and analysis packages. Additionally, the ability to handle the non-uniform wavelength interval at which the spectral computations are made was added. This allowed a precise superposition of wavelengths at which the spectral measurements have been made with the wavelengths at which the spectral computations are done by using the line-by-line (LBL) code.

To account for hydrocarbon combustion products in the plume, which might interfere with detection and quantification of metallic elements in the spectral region of 300 to 850 nm, the spectroscopic code has been enhanced to include the carbon-based combustion species of $C_2$, CO, and CH. In addition, CN and NO have spectral bands in 300 to 850 nm and, while these molecules are not direct products of hydrocarbon-oxygen combustion systems, they can show up if nitrogen or a nitrogen compound is

present as an impurity in the propellants and/or these can form in the boundary layer as a result of interaction of the hot plume with the atmosphere during the ground testing of engines. Ten additional electronic band systems of these five molecules have been included into the code. A comprehensive literature search was conducted to obtain the most accurate values for the molecular and the spectral parameters, including Franck-Cordon factors and electronic transition moments for all ten band systems.

For each elemental transition in the RPSSC, six spectral parameters — Doppler broadened line width at half-height, pressure-broadened line width at half-height, electronic multiplicity of the upper state, electronic term energy of the upper state, Einstein transition probability coefficient, and the atomic line center — are required. Input files have been created for ten elements of Ni, Fe, Cr, Co, Cu, Ca, Mn, Al, Ag, and Pd, which retain only relatively moderate to strong transitions in 300 to 430

nm spectral range for each element. The number of transitions in the input files is 68 for Ni; 148 for Fe; 6 for Cr; 87 for Co; 1 for Ca; 3 for Mn; 2 each for Cu, Al, and Ag; and 11 for Pd.

# Research on Spoken Dialogue Systems
## Human verbal interaction with complex information sources.

*Ames Research Center, Moffett Field, California*

Research in the field of spoken dialogue systems has been performed with the goal of making such systems more robust and easier to use in demanding situations. The term "spoken dialogue systems" signifies unified software systems containing speech-recognition, speech-synthesis, dialogue management, and ancillary components that enable human users to communicate, using natural spoken language or nearly natural prescribed spoken language, with other software systems that provide information and/or services. The research is proceeding on several fronts: recognition of speech signals, syntactic and semantic parsing, language modeling, discourse analysis, and contact modeling.

Many of the advances made thus far in this research have been incorporated into a voice-enabled procedure-browser and reader, called Clarissa, that has been tested aboard the International Space Station. [A procedure-browser and reader is essentially a software version of an instruction manual that may describe one or more possibly complex procedure(s).] Major problems that have been addressed in developing Clarissa include creating voice-navigable versions of formal procedure documents, grammar-based speech recognition, methods for accurate detection of user's speech directed toward a listener other than Clarissa based on grammar filtering or support vector machines, and robust, side-effect-free dialogue management for enabling undoing, correction, and/or confirmation of steps of a procedure.

Clarissa enables the user to navigate a complex procedure using only spoken input and output, making it unnecessary for the user to shift visual attention from the task at hand to a paper instruction manual or to an equivalent document displayed on a computer screen. Clarissa also provides a graphical user interface (GUI) for optional visual display of information. Clarissa has a vocabulary of about 260 words and supports about 75 different commands, including commands for reading steps of the procedure, scrolling forward or backward in the procedure, moving to an arbitrary new step, reviewing noncurrent steps, adding and removing voice notes, displaying pictures, setting and canceling alarms and timers, requiring challenges to verify critical commands, and querying the system as to status of the procedure.

Clarissa includes the following main software modules:
• Speech Processor — Performs low-level speech-recognition (input) and speech-synthesis (output) functions.
• Semantic Analyzer — Converts output from the speech processor into an abstract dialogue move.
• Response Filter — Decides whether to accept or reject the spoken input from the user.
• Dialogue Manager — Converts abstract dialogue moves into abstract dialogue actions, and maintains knowledge of both the context of the discourse and the progress through the procedure.
• Output Manager — Accepts abstract dialogue actions from the Dialogue Manager and converts them into lists of procedure calls that result in concrete system responses, which can in-

clude spoken output, requests for display of visual output on the GUI, or sending dialogue moves back to the Dialogue Manager.
• GUI Module — Mediates conventional keyboard and screen-based interaction with the user and accepts display requests from the Output Manager. This module can also convert keyboard input from the user into dialogue moves, which are sent to the Dialogue Manager.

Another accomplishment of this research has been the development of a targeted-help module that is highly portable in that it can be added to a spoken dialogue system, with minimal application-specific modifications, to make the spoken dialogue system more robust. The targeted-help module is intended, more specifically, for incorporation into a spoken dialogue system in which, as in Clarissa, there is a prescribed spoken language containing a limited number of words. The purpose served by the targeted-help module is to assist an untrained user to learn the prescribed language by providing help messages in response to out-of-coverage users' utterances (that is, users' utterances outside the prescribed language). These messages can be much more informative than "Sorry, I didn't understand" and variants thereof generated by older, less-capable spoken dialogue systems.

The targeted-help module includes two submodules that run simultaneously: a grammar-based recognizer and a statistical language model (SLM). When the grammar-based recognizer succeeds, the ordinarily-less-accurate hypothesis generated by the SLM rec-

ognizer is not used. When the grammar-based recognizer fails and the SLM recognizer produces a recognition hypothesis, the SLM output is processed to generate a message that tells the user what was recognized as having been uttered, a diagnosis of what was problematic about the recognized utterance, and a related in-coverage example. The in-coverage example is intended to encourage alignment between the user's utterances and the prescribed language.

# Injecting Errors for Testing Built-in Test Software

*Lyndon B. Johnson Space Center, Houston, Texas*

Two algorithms have been conceived to enable automated, thorough testing of Built-in test (BIT) software. The first algorithm applies to BIT routines that define pass/fail criteria based on values of data read from such hardware devices as memories, input ports, or registers. This algorithm simulates effects of errors in a device under test by (1) intercepting data from the device and (2) performing AND operations between the data and the data mask specific to the device. This operation yields values not expected by the BIT routine. This algorithm entails very small, permanent instrumentation of the software under test (SUT) for performing the AND operations.

The second algorithm applies to BIT programs that provide services to users' application programs via commands or callable interfaces and requires a capability for test-driver software to read and write the memory used in execution of the SUT. This algorithm identifies all SUT code execution addresses where errors are to be injected, then temporarily replaces the code at those addresses with small test code sequences to inject latent severe errors, then determines whether, as desired, the SUT detects the errors and recovers.

# Guidance and Control System for a Satellite Constellation

*Goddard Space Flight Center, Greenbelt, Maryland*

A distributed guidance and control algorithm was developed for a constellation of satellites. The system repositions satellites as required, regulates satellites to desired orbits, and prevents collisions.
1. Optimal methods are used to compute nominal transfers from orbit to orbit.
2. Satellites are regulated to maintain the desired orbits once the transfers are complete.
3. A simulator is used to predict potential collisions or near-misses.
4. Each satellite computes perturbations to its controls so as to increase any unacceptable distances of nearest approach to other objects.
   a. The avoidance problem is recast in a distributed and locally-linear form to arrive at a tractable solution.
   b. Plant matrix values are approximated via simulation at each time step.
   c. The Linear Quadratic Gaussian (LQG) method is used to compute perturbations to the controls that will result in increased miss distances.
5. Once all danger is passed, the satellites return to their original orbits, all the while avoiding each other as above.
6. The delta-Vs are reasonable. The controller begins maneuvers as soon as practical to minimize delta-V.
7. Despite the inclusion of trajectory simulations within the control loop, the algorithm is sufficiently fast for available satellite computer hardware.
8. The required measurement accuracies are within the capabilities of modern inertial measurement devices and modern positioning devices.

# Books & Reports

## ⚙ Dedicated Deployable Aerobraking Structure

A dedicated deployable aerobraking structure concept was developed that significantly increases the effective area of a spacecraft during aerobraking by up to a factor of 5 or more (depending on spacecraft size) without substantially increasing total spacecraft mass. Increasing the effective aerobraking area of a spacecraft (without significantly increasing spacecraft mass) results in a corresponding reduction in the time required for aerobraking. For example, if the effective area of a spacecraft is doubled, the time required for aerobraking is roughly reduced to half the previous value. The dedicated deployable aerobraking structure thus enables significantly shorter aerobraking phases, which results in reduced mission cost, risk, and allows science operations to begin earlier in the mission.

In order to achieve a large area without impacting the spacecraft or launch vehicle, a deployable structure is necessary. The dedicated deployable aerobraking structure uses a set of deployable rigid "arms" to deploy and support a large membrane. The membrane is made of material (Kapton, for example) that can withstand the thermal and mechanical loads characteristic of aerobraking. Once aerobreaking is complete, this aerobraking structure would be jettisoned into an atmosphere-intercepting orbit and subsequently destroyed upon atmospheric entry. This concept uses a mechanical implementation distinct from inflatable aerodynamic decelerators studied for aerocapture and other applications. Aerobraking requires multiple passes through the atmosphere over several weeks (at least), and so any small leaks or punctures that develop in an inflatable structure during that time could compromise the inflatable structure; this makes inflatable structures a higher risk implementation for an aerobraking structure relative to the mechanical implementation used in this concept.

Tentative mechanical and thermal requirements for this technology have been developed. Full-scale proof of concept hardware corresponding to one quadrant of a 72 $m^2$ aerobraking structure was successfully designed, fabricated, deployed, and tested. The lab tests were designed so that the mechanical loads in the 1-g lab environment were higher than the anticipated aerobraking loads, which proved the structure could survive in flight. Finite element models were developed and found to be in good agreement with the proof-of-concept hardware. Thermal and attitude stability aspects of the concept were analyzed. Based on the preliminary requirements, hardware tests, computational models, and analyses developed, the concept was found to be viable using conventional engineering materials and techniques.

In addition to potential use on planetary missions, this technology can also be used as an inexpensive, robust, and reliable method for reducing orbital debris hazards in Earth orbit by increasing the rate of orbital decay of objects in orbit about the Earth such as decommissioned satellites and spent launch vehicle upper stages.

*This work was done by Louis R. Giersch and Kevin Knarr of Caltech for NASA's Jet Propulsion Laboratory. Further information is contained in a TSP (see page 1). NPO-47227*

## Σ Portable Health Algorithms Test System

A document discusses the Portable Health Algorithms Test (PHALT) System, which has been designed as a means for evolving the maturity and credibility of algorithms developed to assess the health of aerospace systems. Comprising an integrated hardware-software environment, the PHALT system allows systems health management algorithms to be developed in a graphical programming environment, to be tested and refined using system simulation or test data playback, and to be evaluated in a real-time hardware-in-the-loop mode with a live test article.

The integrated hardware and software development environment provides a seamless transition from algorithm development to real-time implementation. The portability of the hardware makes it quick and easy to transport between test facilities. This hardware/software architecture is flexible enough to support a variety of diagnostic applications and test hardware, and the GUI-based rapid prototyping capability is sufficient to support devel-opment, execution, and testing of custom diagnostic algorithms.

The PHALT operating system supports execution of diagnostic algorithms under real-time constraints. PHALT can perform real-time capture and playback of test rig data with the ability to augment/modify the data stream (e.g. inject simulated faults). It performs algorithm testing using a variety of data input sources, including real-time data acquisition, test data playback, and system simulations, and also provides system feedback to evaluate closed-loop diagnostic response and mitigation control.

*This work was done by Kevin J. Melcher and Edmond Wong of Glenn Research Center and Christopher E. Fulton, Thomas S. Sowers, and William A. Maul of Analex Corp. Further information is contained in a TSP (see page 1).*

*Inquiries concerning rights for the commercial use of this invention should be addressed to NASA Glenn Research Center, Innovative Partnerships Office, Attn: Steve Fedor, Mail Stop 4–8, 21000 Brookpark Road, Cleveland, Ohio 44135. Refer to LEW-18485-1.*

## Σ Technique for Performing Dielectric Property Measurements at Microwave Frequencies

A paper discusses the need to perform accurate dielectric property measurements on larger sized samples, particularly liquids at microwave frequencies. These types of measurements cannot be obtained using conventional cavity perturbation methods, particularly for liquids or powdered or granulated solids that require a surrounding container. To solve this problem, a model has been developed for the resonant frequency and quality factor of a cylindrical microwave cavity containing concentric cylindrical samples. This model can then be inverted to obtain the real and imaginary dielectric constants of the material of interest.

This approach is based on using exact solutions to Maxwell's equations for the resonant properties of a cylindrical microwave cavity and also using the effective electrical conductivity of the cavity walls that is estimated from the measured empty cavity quality factor. This new approach calculates the complex resonant frequency and associated electromagnetic fields for a cylindrical mi-

crowave cavity with lossy walls that is loaded with concentric, axially aligned, lossy dielectric cylindrical samples. In this approach, the calculated complex resonant frequency, consisting of real and imaginary parts, is related to the experimentally measured quantities.

Because this approach uses Maxwell's equations to determine the perturbed electromagnetic fields in the cavity with the material(s) inserted, one can calculate the expected wall losses using the fields for the loaded cavity rather than just depending on the value of the fields obtained from the empty cavity quality factor. These additional calculations provide a more accurate determination of the complex dielectric constant of the material being studied. The improved approach will be particularly important when working with larger samples or samples with larger dielectric constants that will further perturb the cavity electromagnetic fields. Also, this approach enables the ability to have a larger sample of interest, such as a liquid or powdered or granulated solid, inside a cylindrical container.

*This work was done by Martin B. Barmatz of Caltech and Henry W. Jackson for NASA's Jet Propulsion Laboratory. Further information is contained in a TSP (see page 1).*

National Aeronautics and
Space Administration